People's Democratic Republic of Algeria
Ministry of Higher Education and Scientific Research

University M'HAMED BOUGARA – Boumerdes

Institute of Electrical and Electronic Engineering

Department of Electronics

Final Year Project Report Presented in Partial Fulfilment of the Requirements for the Degree of

'MASTER'

In ***Telecommunications***

Option: ***Telecommunications***

Title:

Gain Enhancement of Microstrip Antenna Using Artificial Magnetic Conductor

Presented by:

- **HAMRIOUI Fatma Zohra**
- **BOUHAFS Djazia**

Supervisor:

Pr. A. AZRAR

Registration Number:……/2020

Acknowledgements

First and foremost, we would like to thank Almighty ALLAH for giving us the courage and the determination, as well as guidance in conducting this project study, despite the difficulties.

Our sincere thanks and gratitude goes to our supervisor and principal lecturer "Pr. AZRAR", for his support, guidance and encouragement during this project. His positive outlook and confidence in our project inspired us and gave us confidence. His careful editing contributed enormously to accomplish this work.

We would like to express our sincere gratitude to Mrs. MOUHOUCHE, for the help and the support she provided during this research work. Special thanks to Mrs.MEHENNAOUI the head of library and all the staff of IGEE institute Library who are always ready whenever we need their help.

Next, we owe a special thanks to the members of the jury who have agreed to evaluate our work.

Last but not least, many thanks go to the institute's teachers who have encouraged and taught us in our five-year program and to all those who have contributed directly or indirectly to our five-year journey to the institute.

Dedication

To the one who held my hand so that I did not fall,

My precious Dad,

To the one who surrounded me with warmth and love so that I kept being strong

Beloved Mom.

Thanks so much for your love and support throughout my life. Thanks again for your encouragement and endless sacrifices.

To my lovely sisters and my dear brother for supporting me all the time.

*To my niece "**Anfel** "my little princess, I love you to the moon and back.*

To all my friends who have never left my side specially Kenza, Lillia, Lydia and Amina.

To all who were there for me

To my childhood and to each moment I lived to reach this day.

I dedicate this work.

F. Zahra

Dedication

Every challenging work needs self efforts as well as guidance of olders especially those who were very close to our heart.

I dedicate this humble project to the strongest and most powerful woman I have ever seen, my wonderful and lovely mother ***SOUHILA****, thank you for your unconditional support and courage in all my path of my studies.*

A special dedication to the memory of my father ***ABD EL FETTEH,*** *to my adorable sisters Aya and Asma and her husband Billel without forgetting the sweet angels of the family Emily and Assil.*

I also dedicate this work to the families Bouhafs, Yahi, Hadjout, Hallej and Alouache and to my dear friends Yousra, Amina, Sousou and Karim. I'm grateful to have you in my life and I wish you the best of your life.

Djazia

Abstract

A dual band CPW microstrip antenna over an artificial magnetic conductor (AMC) is presented in this work. The AMC surface is designed as a dual band reflector to enhance the antenna gain. The effect of varying the antenna-reflector distance on the antenna performance is studied. Initially, a microstrip antenna with new form is designed to operate at 2.45 GHz and 5.2 GHz simultaneously to cover the WLAN application with a good impedance matching and low realized gain of 2.27 dBi and 2.22 dBi respectively. Then, a new AMC unit cell is constructed to investigate a reflection phase bands, from $-90°$ to $+90°$, centered at 2.484 GHz and 5.204 GHz. Finally, the CPW antenna is loaded with an AMC surface of 6×6 units and an analysis of the antenna-AMC distance impact is done. It is found that the variation in the distance affects the antenna performances. The evaluation results from the comparison between the AMC antenna and the reference antenna indicate that an improvement in directivity and radiation patterns is achieved and the gain enhancement can be up to more than 5 dBi.

List of Abbreviations

CPW	Co-Planar Waveguide
MTMs	Metamaterials
RHM	Right Hand Medium
LHM	Left Hand Medium
DPS	Double Positive
ENG	Epsilon Negative
MNG	Mu Negative
SRR	Split Ring Resonator
DNG	Double Negative
NIM	Negative refractive Index Metamaterial
EBG	Electromagnetic Band Gap
FSS	Frequency Selective Surface
HIS	High Impedance Surfaces
AMC	Artificial Magnetic Conductor
PEC	Perfect Electric Conductor
PMC	Perfect Magnetic Conductor
CST	Computer Simulation Technology
FR-4	Flame Resistant 4
WLAN	Wireless Local Area Network
VSWR	Voltage Standing Wave Ratio
GPS	Global Positioning System
GSM	Global System for Mobile Communication

Table of Contents

Acknowledgements i
Dedication ii
Dedication iii
Abstract iv
List of Abbreviations v
List of Figures viii
List of Tables x
General Introduction 1
CHAPTER 01: Generalities about Microstrip Antenna and Metamaterials 3
1.1 Introduction 3
1.2 Microstrip Antenna 3
1.2.1 History 3
1.2.2 Basic Structure 3
1.2.3 Principle of Operation of Microstrip Antenna 4
1.2.4 Feeding Techniques 4
1.2.4.1 Microstrip Line Feed 5
1.2.4.2 Coaxial Feed 5
1.2.4.3 Aperture Coupled Feed 5
1.2.4.4 Proximity Coupled Feed 5
1.2.5 Antenna Parameters and Characteristics 6
1.2.5.1 Impedance Bandwidth 6
1.2.5.2 Input Impedance 6
1.2.5.3 Directivity 6
1.2.5.4 Efficiency 7
1.2.5.5 Gain and Realized Gain 7
1.2.5.6 Radiation Pattern 7
1.2.5.7 Polarization 7
1.3 Metamaterials 8
1.3.1 The Properties Of Metamaterials 8
1.3.2 Classification of Metamaterials 9
1.3.2.1 Double Positive (DPS) Material 9
1.3.2.2 Epsilon Negative (ENG) Metamaterial 9
1.3.2.3 Mu Negative (MNG) Metamaterial 10
1.3.2.4 Double Negative (DNG) Metamaterial 11
1.3.3 Metamaterials Types 11
1.3.3.1 Electromagnetic Band Gap (EBG) Metamaterials 11

1.3.3.2 Frequency Selective Surface (FSS) Based Metamaterials 12
1.3.3.3 Artificial Magnetic Conductor (AMC) 13
1.4 Conclusion 14
CHAPTER 02: Design of Dual Band Microstrip Antenna 15
2.1 Introduction 15
2.2 Design of Dual-Band Microstrip Antenna 15
2.3 Simulation and Results 15
2.3.1 Parametric Study of the Proposed CPW Antenna 16
2.3.2 Voltage Standing Wave Ratio 19
2.3.3 Current Distribution 20
2.3.4 Radiation Pattern 20
2.3.5 Antenna Efficiency 22
2.3.6 Gain and Directivity 23
2.4 Conclusion 23
CHAPTER 03: Design of Dual Band AMC Unit Cell 24
3.1 Introduction 24
3.2 Design of Dual Band AMC Unit Cell 24
3.3 Simulation and Results 24
3.3.1 Parametric Study of the Proposed AMC Unit Cell 25
3.3.2 Surface Impedance 29
3.3.3 Current distribution 30
3.3.4 Periodic structure 30
3.4 Conclusion 32
CHAPTER 04: Gain Enhancement Using High Impedance Surface 33
4.1 Introduction 33
4.2 Monopole antenna loaded with AMC surface 33
4.3 Simulation and Results 33
4.3.1 Distance impact on The Antenna Performance 33
4.3.2 AMC Size Impact on the Antenna Performance 36
4.2.3 The Optimum Design for Monopole Antenna Loaded With AMC Surface 38
4.4 Conclusion 42
Conclusions and Suggestions for Further Work 43
References xi
APPENDIX A: Coplanar Line xiii
A.1 Definition xiii
A.2 Characteristic Impedance and Effective Permittivity xiii
A.3 Designing Coplanar Line xiv

List of Figures

Figure 1.1 Structure of microstrip antenna 3
Figure 1.2 Basic shapes of Microstrip patch antenna 4
Figure 1.3 Electric field lines in microstrip antennas. 4
Figure 1.4 Feeding techniques of microstrip antennas,**(a)** Microstrip Line Feed, **(b)** Coaxial Feed, **(c)** Aperture Coupled Feed **(d)** Proximity Coupled Feed. 5
Figure 1.5 The vectors E,H and k form (a) right hand media (b) left handed media. 9
Figure 1.6 The classification of electromagnetic MTMs based on signs of the ε and μ. 9
Figure 1.7 An array of thin conducting wires **(a),** plots of the effective permittivity of an array of wires **(b)**. 10
Figure 1.8 An array of SRRs **(a)**, the effective permeability of SRR array **(b).** 10
Figure 1.9 Combination of thin wires and SRR to form DNG metamaterials 11
Figure 1.10 Examples of realizations of DNG metamaterials **(a)** and **(b)**. 11
Figure 1.11 Types of electromagnetic bandgaps based on geometrical shapes, **(a)**1D **(b)** 2D **(c)** 3D. 12
Figure 1.12 Two examples of metallic FSSs, **(a)** Slot array on a dielectric sheet (**b)** Dipole array on a dielectric sheet. 12
Figure 1.13 A radiator lying flat against, **(a)** PEC **(b)** a Metamaterial AMC. 14
Figure 2.1 Geometry and dimensions of CPW-fed triangular ring microstrip antenna,(a) Top view (b) Side view 15
Figure 2.2 Ungrounded coplanar port size. 16
Figure 2.3 Simulated input impedance for full triangle and slotted triangle structure, **(a)** Re (Zin) (**b)** Im (Zin) 17
Figure 2.4 Effect of varying the patch height and width on the input reflection coefficient **(a)** effect of the patch height, L **(b)** effect of the patch width, W. 17
Figure 2.5 Effect of varying the slot height and width on the input reflection coefficient,**(a)**effect of the slot height, l **(b)** effect of the slot width, w. 18
Figure 2.6 Effect of varying the gap between the patch and the ground and feed-line on the input reflection coefficient, **(a)**effect of the gap, G **(b)** effect of the feed line width, W_f. 18
Figure 2.7 Simulated input reflection coefficient of the dual band CPW antenna 19
Figure 2.8 Simulated input VSWR of the dual band CPW antenna. 19
Figure 2.9 The current distribution of the CPW antenna at **(a)** 2.45GHz, **(b)** 5.20 GHz. 20
Figure 2.10 Simulated radiation patterns of the proposed Antenna at 2.45 GHz, (a) Co-polar components (b) Cross-polar components. 21
Figure 2.11 Simulated radiation patterns of the proposed Antenna at 5.20 GHz,(a)Co-polar components(b)Cross-polar components. 21
Figure 2.12 Simulated 3D radiation patterns of the proposed Antenna. **(a)** pattern at 2.45GHz **(b)** pattern at 5.20 GHz. 22
Figure 2.13 Antenna efficiency versus frequency of the CPW antenna 22
Figure 2.14 the simulated gains and directivity versus frequency of the CPW antenna. 23
Figure 3.1 Geometry and dimensions of AMC unit cell, (a) Top view (b) Side view 24
Figure 3.2 Boundary conditions setup of the proposed AMC unit cell. 25
Figure 3.3 Boundary conditions methodology for the proposed AMC unit cell 25
Figure 3.4 Reflection phase of the AMC unit cell at different stages 26
Figure 3.5 Effect of varying the length q on reflection phase. 26
Figure 3.6 Effect of varying r on reflection phase. 27

Figure 3.7 Effect of varying k on reflection phase. 27
Figure 3.8 Effect of varying s on reflection phase. 28
Figure 3.9 Effect of varying i on reflection phase. 28
Figure 3.10 Reflection phase response for proposed AMC unit cell. 29
Figure 3.11 Surface impedance of the dual band AMC unit cell. 30
Figure 3.12 Current distribution of the dual band AMC unit cell at, (a) 2.45GHz **(b)** 5.20GHz. 30
Figure 3.13 Reflection phase of different AMC surface size. 31
Figure 3.14 Surface impedance of the 6 by 6 AMC structure. 31
Figure 3.15 Current distribution of the 6 by 6 AMC structure at, (**a)** 2.45 GHz (**b)** 5.20 GHz. 32
Figure 4.1 Configuration of CPW antenna with an AMC reflector**, (a)** top view **(b)** Side view. 33
Figure 4.2 Simulated realized gain and directivity versus distance. 34
Figure 4.3 Simulated efficiency versus distance at **(a)** 2.45 GHz (**b)** 5.2 GHz. 34
Figure 4.4 Simulated radiation patterns at 2.45 GHz, **(a)** E plane **(b)** H plane 35
Figure 4.5 Simulated radiation patterns at 5.2 GHz, **(a)** E plane **(b)** H plane. 35
Figure 4.6 Simulated input reflection coefficient of the CPW antenna at different distances from the AMC surface. 36
Figure 4.7 Simulated input reflection coefficient for the monopole antenna for different sizes of AMC surface. 36
Figure 4.8 Simulated radiation patterns for different sizes of AMC surface at 2.45 GHz, **(a)** E plane **(b)** H plane. 37
Figure 4.9 Simulated radiation patterns for different sizes of AMC surface at 5.2GHz,(a) E plane **(b)** H plane. 37
Figure 4.10 Simulated input reflection coefficient for the monopole antenna with and without AMC surface. 38
Figure 4.11 Simulated radiation patterns of the CPW antenna with and without AMC surface at 2.45 GHz, **(a)** E plane **(b)** H plane. 39
Figure 4.12 Simulated radiation patterns of the CPW antenna with and without AMC surface at 5.2 GHz, **(a)** E plane (**b)** H plane. 39
Figure 4.13 Simulated 3D radiation patterns of the CPW antenna over AMC surface at **(a)** 2.45GHz (**b)** 5.20 GHz. 40
Figure 4.14 The current distribution of the CPW antenna over AMC surface at **(a)** 2.45GHz **(b)** 5.20 GHz. 40
Figure 4.15 Antenna efficiency versus frequency of the CPW antenna over AMC surface. .. 41
Figure 4.16 Simulated input reflection coefficient for various cases. 41
Figure A.1 (a) Geometry of a coplanar transmission line **(b)** electric and magnetic field distribution of a quasi-TEM wave. xiii
Figure A.2 The characteristic impedance $Z0$ versus the ratio wd xv
Figure A.3 The width of coplanar strip line versus slot width for $Z0 = 50\ \Omega$ xv
Figure A.4 Impedance coplanar waveguide calculation. xv

List of Tables

Table 2.1 The dimensions of the CPW triangular ring microstrip antenna 15
Table 3.1 the dimensions of AMC unit cell. 24
Table 4.1 Simulated results ofthe antenna over different sizes of AMC surface at 2.45 GHz. 37
Table 4.2 Simulated results of the antenna over different sizes of AMC surface at 5.2 GHz. 38
Table 4.3 Simulated antenna performances at 2.45 GHz and 5.20 GHz..... 42

General Introduction

General Introduction

In the recent years, the most important challenges for system designers are the low cost, minimal weight and low profile to accomplish in the design and performance enhancement of each wireless component such as antenna. The antenna is the heart of every wireless communication system ;it ensures the reception and transmission of radio wave signals from and into the air. It has different types such as microstrip antenna that has most innovative field engineering thanks to its low material cost and manufacturing ease.

Microstrip antennas are widely used nowadays starting from the modern communication systems to pacemaker device. Depending on the type of application, microstrip antennas are designed to achieve particular performance. One of these applications is Wireless local area network (WLAN) which assigns two separate indoor WLAN frequencies. The first is at 2.4 GHz, and the second at 5.2 GHz. Those two different frequencies require two single band antennas. However the solution can be done with just one antenna, by designing a dual band microstrip antenna to cover WLAN (2.4 GHz, 5.2 GHz).

However, the design of a micorstrip antenna is not always an easy problem and the designer faces some of its drawbacks such as a narrow bandwidth, low gain and surface wave excitation that reduces the radiation efficiency. To overcome the gain and efficiency a new design methodology is used which is an artificially created structure called metamaterial.

Metamaterial is an artificial resonant structure designed to obtain a specific characteristics that are not naturally occurring in nature [1]. These unique characteristics of metamaterials have been widely used in antennas and microwave applications to improve the desired performance [2].Artificial magnetic conductor AMC is sub classes of metamaterials that is designed to imitate the behavior of the perfect magnetic conductor PMC that is not existed in nature. This type of metamaterials introduces an in phase reflection at the desired frequency and has been widely used as an artificial ground plane or reflector to enhance the performance of many different antenna types while achieving profile miniaturization [3].

The aim of this project is to design a dual band monopole antenna based on AMC reflector. In contrast to many studies on single band low profile antenna design; the work focuses on improving the radiation performance of CPW monopole antenna within two operating bands simultaneously which is typically a challenge due to the mutual influence between the antenna and the AMC surface.

Contributions and project organization

The project is arranged into four chapters:
Chapter 1 provides generalities on microstrip antenna including a short review of microstrip antenna history, various feeding forms and antenna parameters and characteristics. On the other hand, the topic of metamaterials is briefly discussed on the properties, different classes and types of metamaterials such as EBG, FSS and AMC surfaces.

Chapter 2 discusses the dual band monopole antenna that is used to cover WLAN applications (2.4 GHz, 5.2 GHz). The geometry of the proposed design is clearly explained by showing the effect of various parameters on the antenna performance. Then, different antenna

characteristics are simulated using computer simulation technology CST, such as the input reflection coefficient, input impedance, voltage standing wave ratio, efficiency, directivity and gain . The current distribution and radiation patterns are shown at both resonant frequencies.

Chapter 3 presents the dual band artificial magnetic conductor (AMC) unit cell design that is used to operate at 2.45 GHz and 5.2 GHz. A comparative study is done on the effect of various parameters on the reflection phase to understand the construction of the AMC unit cell. Then the surface impedance and current distribution are simulated and explained. Furthermore, distinct sizes of periodic AMC structure are investigated and simulated in the last section of this chapter.

Chapter 4 presents the design and study of the proposed dual band monopole antenna loaded with periodic AMC surface. The first and second parts deal with the distance and AMC size impact on the antenna performance. In the last part, the characteristics of the optimum AMC antenna are simulated and compared with the reference antenna to show the improvement in gain and directivity.

This work ends with conclusions and some suggestions for further research.

CHAPTER 01

Generalities about Microstrip Antenna and Metamaterials

CHAPTER 01: Generalities about Microstrip Antenna and Metamaterials

1.1 Introduction

Microstrip antennas have become one of the most common types of antennas in the telecommunications industry today due to their low profile, light weight and ease of fabrication. Their innovative designs will keep playing a significant role in the future of wireless devices, however low gain and low bandwidth are a limitation of microstrip antenna. Therefore the concept of metamaterials is used along with microstrip antenna to enhance those features .This material is an engineered material with some decent properties that are generally not found in nature. Thanks to its potential to implement microwave devices with these extraordinary properties, a new area of wireless application has been created.

Before entering into the project details, let us describe in this chapter some useful concepts on microstrip antenna, its behavior and the theory behind metamaterials.

1.2 Microstrip Antenna

1.2.1 History

Microstrip Antenna was initially proposed by Deschamps in 1953 [4] .In 1955, a patent right was won by Vaissinot and Gutton.The general characteristics of travelling waves microstrip antennas were discussed extensively by Jasik in 1961,Walter in 1965 and Collins and Zucker in 1969.In the early year of 1970, a practical implementation was done by Howell and Munsoon [5].The conventional shaped microstrip antennas such as rectangular and circular disk are studied extensively by Demeryd in 1978 and 1979.

1.2.2 Basic Structure

A microstrip patch antenna consists of a conducting patch of any non-planar or planar geometry on one side of a dielectric substrate and a ground plane on other side as shown in Figure1.1[6].

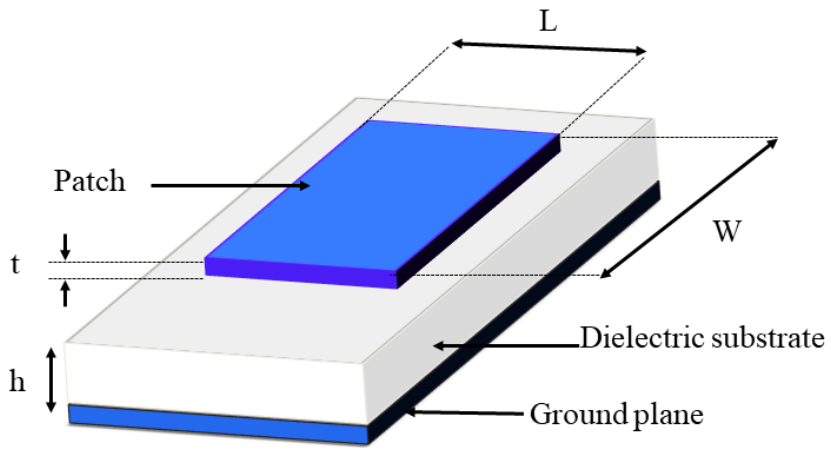

Figure 1.1 Structure of microstrip antenna.

These antennas can be made of various designs according to the use. The basic configurations used in practice are shown in Figure 1.2 [4].

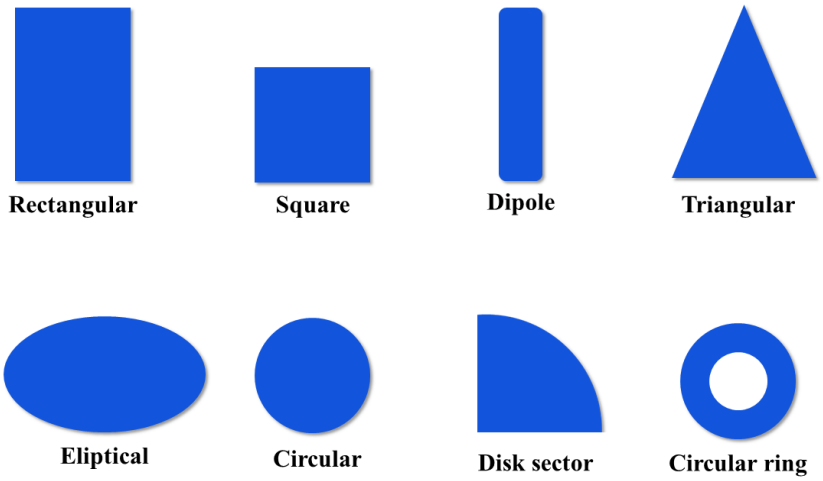

Figure 1.2 Basic shapes of Microstrip patch antenna.

1.2.3 Principle of Operation of Microstrip Antenna

Microstrip antenna is a transducer which transmits or receives electromagnetic waves. Figure 1.3 shows the field lines in an non-homogenous medium composed generally by air and substrate. Typically most of the field lines lie in the substrate and parts exit in air. Since part of the waves travel in the substrate and part in air, an effective dielectric constant ε_{eff} is introduced to account for fringing and wave propagation in the line [7]. Therefore, the performances of the microstrip patch sensor will be affected by effective dielectric constant ε_{eff} of the substrate and the dimension of patch .

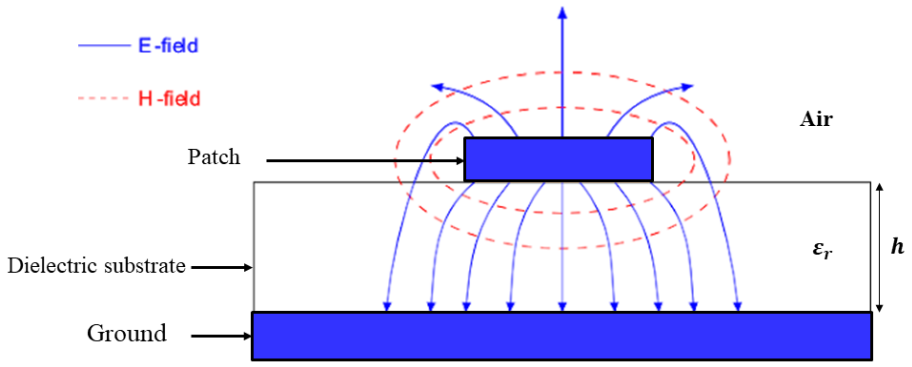

Figure 1.3 Electric field lines in microstrip antennas.

Fringing effect comes due to electric field lines which makes the antenna size wider after excitation. The main cause of fringing effect is due to width and position of feed in antenna, and it‘s the responsible of the radiation mechanism and give more directive radiation pattern but resonant frequency is shifted from the desired frequency.

1.2.4 Feeding Techniques

Microstrip patch antennas can be fed with many methods but the four most popular feeding techniques used are Microstrip Line Feed, Coaxial Feed, Aperture Coupled Feed and Proximity Coupled Feed as shown in figure 1.4 [8].

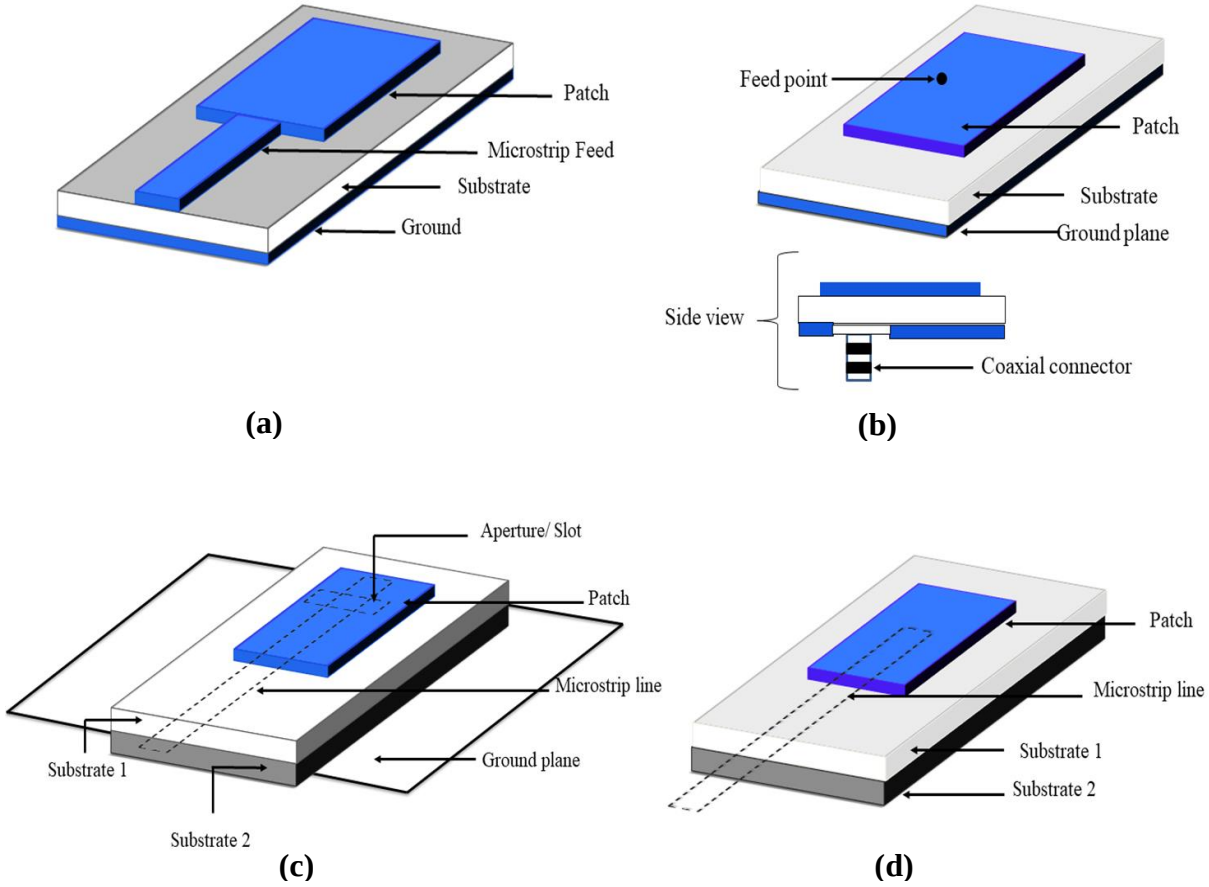

Figure 1.4 Feeding techniques of microstrip antennas,
(a) Microstrip Line Feed, **(b)** Coaxial Feed, **(c)** Aperture Coupled Feed **(d)** Proximity Coupled Feed.

1.2.4.1 Microstrip Line Feed

A conducting strip is connected directly to the edge of the microstrip patch. The conducting strip is smaller in width as compared to the patch.

1.2.4.2 Coaxial Feed

The inner conductor of the coaxial connector extends throughout the dielectric and is soldered to the radiating patch, while the outer conductor is coupled to the ground plane.

1.2.4.3 Aperture Coupled Feed

The radiating patch and the microstrip feed line are separated by the ground plane. The patch and the feed line are coupled through a slot in the ground plane. The coupling slot is centered below the patch, leading to low cross polarization due to symmetry of the configuration. Since the ground plane separates the patch and the feed line, spurious radiation is minimized.

1.2.4.4 Proximity Coupled Feed

Two dielectric substrates are used and the feed line is between them. The radiating patch is on the top of the upper substrate.

1.2.5 Antenna Parameters and Characteristics

To describe the performance of an antenna, definitions of various parameters are necessary.

1.2.5.1 Impedance Bandwidth

The impedance bandwidth describes the bandwidth over which the antenna has acceptable losses due to mismatch. The impedance bandwidth can be measured by the characterization of both the voltage standing wave ratio (VSWR) and return loss (RL) at the frequency band of interest. Both VSWR and RL are dependent on measuring the reflection coefficient Γ at the terminals of the antenna that is defined by **[**9**]**:

$$\Gamma = \frac{Z_{in}-Z_0}{Z_{in}+Z_0} \quad (1\text{-}1)$$

Where Z_{in} is the antenna input impedance and Z_0 is the feeding line /probe characteristic impedance.
The VSWR is defined as the ratio between the voltage maximum and voltage minimum of the standing wave created by the mismatch at the load on a transmission line **[**9**]**. The VSWR equation is shown in Equation 1.2.

$$VSWR = \frac{1+|\Gamma|}{1-|\Gamma|} \quad (1\text{-}2)$$

the return loss is defined as the ratio of the power incident on the antenna P_{in} to the power reflected back from the antenna P_r.Therefore the higher the ratio is, the better the antenna is matched. And is defined in dB as **[**9**]**:

$$RL = -20log|\Gamma| \quad (1\text{-}3)$$

1.2.5.2 Input Impedance

The input impedance is an important consideration to have of better result of an antenna granted on a transmitter or a receiver. By definition, the input impedance of an antenna is the impedance presented by an antenna at its terminals or the ratio of the voltage current at a pair of terminals. It is given by the following formula [10]:

$$Z_{in} = Z_0 \frac{1+\Gamma}{1-\Gamma} \quad (1\text{-}4)$$

1.2.5.3 Directivity

Directivity of an antenna is defined as the ratio of the radiation intensity in a given direction from the antenna to the radiation intensity averaged over all directions. The average radiation intensity is equal to the total power radiated by the antenna divided by 4π.Stated more simply; the directivity of a non isotropic source is equal to the ratio of its radiation intensity in a given direction over that of an isotropic source [11].

$$D = \frac{U}{U_0} = \frac{4\pi U}{P_{rad}} \quad (1\text{-}5)$$

Where D is the directivity, U is the radiation intensity, U_0 is the radiation intensity of isotropic source and P_{rad} is the total radiated power.
If the direction is not specified, it implies the direction of maximum radiation intensity (maximum directivity) expressed as [11]:

$$D_{max} = \frac{U_{max}}{U_0} = \frac{4\pi U_{max}}{P_{rad}} \quad (1\text{-}6)$$

Where D_{max} is the maximum directivity and U_{max} is the maximum radiation intensity.

1.2.5.4 Efficiency

Antenna efficiency is a useful and informative measure of antenna. The total antenna efficiency is used to take into account losses at the input terminals and within the structure of the antenna. Such losses may be due to reflections because of the mismatch between the transmission line and the antenna and I ^{2}R losses (conduction and dielectric).
In general, the overall efficiency can be written as [11]:

$$e_0 = e_r e_{cd} \quad (1\text{-}7)$$

Where e_0 is the total efficiency, e_{cd} is the conduction and dielectric efficiency and also known as radiation efficiency and e_r is the reflection efficiency and it's given by:

$$e_r = (1 - |\Gamma|^2) \quad (1\text{-}8)$$

1.2.5.5 Gain and Realized Gain

Gain of an antenna is defined as the ratio of the intensity in a given direction, to the radiation intensity that would be obtained if the power accepted by the antenna were radiated isotropically. The radiation intensity corresponding to the isotropically radiated power is equal to the power accepted (input) by the antenna divided by 4π. In equation form this can be expressed as [11]:

$$G = \frac{4\pi U}{P_{in}} \quad (1\text{-}9)$$

Where $G$is the Gain, U is the radiation intensity and p_{in} is the total input power.

The gain is a measure that takes into account the radiation efficiency of the antenna as well as its directional capabilities and it can be written as [11]:

$$G = e_{cd} \times D \quad (1\text{-}10)$$

Another type of gain is defined in this part which referred to as realized gain ($\boldsymbol{G_{re}}$), that also takes into account the reflection/mismatch losses and it is given by [11]:

$$G_{re} = e_r \times G \quad (1\text{-}11)$$

Where $\boldsymbol{e_r}$ is the reflection efficiency.

1.2.5.6 Radiation Pattern

An antenna radiation pattern or antenna pattern is defined as a mathematical function or graphical representation of the radiation properties of the antenna as a function of the space parameters. In most cases the radiation pattern is determined in the far field region. Radiation properties include power flux density, radiation intensity, field strength, directivity phase or polarization [12].Performance of the antenna is often described in terms of its principal E- and H- plane patterns.

a. The E-plane pattern

It is defined as the plane containing the electric field vector and the direction of maximum radiation.

b. The H-plane pattern

It is defined as the plane containing the magnetic field vector and the direction of maximum radiation.

1.2.5.7 Polarization

Polarization of an antenna in a given direction is defined as the polarization of the wave transmitted (radiated) by the antenna. Polarization can be classified as linear, circular or elliptical.

❖ **Parasitic components of polarization**

An antenna is said to have good polarization purity if the level of the cross-polarization component, noted E_{cross}, is at least –20 dB lower than the co-polar component, noted Eco[12]. The Ludwing definition of the two components of an antenna polarized along the Oy axis gives

$$\begin{bmatrix} Eco \\ Ecross \end{bmatrix} = \begin{bmatrix} +sin\varphi & +cos\varphi \\ +cos\varphi & -sin\varphi \end{bmatrix} \begin{bmatrix} E_\theta \\ E_\varphi \end{bmatrix} \quad (1\text{-}12)$$

If the antenna is polarized along the Ox axis, the Eco and Ecross are expressed as:

$$\begin{bmatrix} Eco \\ Ecross \end{bmatrix} = \begin{bmatrix} +cos\varphi & -sin\varphi \\ +sin\varphi & +cos\varphi \end{bmatrix} \begin{bmatrix} E_\theta \\ E_\varphi \end{bmatrix} \quad (1\text{-}13)$$

1.3 Metamaterials

1.3.1 The Properties of Metamaterials

The electromagnetic property of these metamaterials can be described by the Maxwell's equations. The transformation of this equation serves to highlight the properties of metamaterials. They are given in the set of equations:

$$\nabla \times \vec{E} = -j\omega\mu\vec{H} \quad (1\text{-}14)$$

$$\nabla \times \vec{H} = j\omega\varepsilon\vec{E} \quad (1\text{-}15)$$

Where $\vec{E}$ and $\vec{H}$ are the vectors of electric and magnetic fields strengths, respectively. ε and μ are the material permittivity and permeability, ω is an angular frequency and $j = \sqrt{-1}$ is an imaginary number.

In the case of the plane wave propagation, the electric and magnetic fields are represented as:

$$\vec{E} = E_0 e^{j(\omega t - kr)} \quad (1\text{-}16)$$

$$\vec{H} = H_0 e^{j(\omega t - kr)} \quad (1\text{-}17)$$

In addition, to evaluate the properties of materials, a general definition of the Poynting power density vector $\vec{S}$ is mentioned, which is subdivided into the time $e^{j\omega t}$ and the space e^{jkr} components. The real part of the Poynting vector $\vec{S}$ which determines the energy flow, is represented by the following formula:

$$\vec{S} = \frac{1}{2}\vec{E} \times \overrightarrow{H^*} \quad (1\text{-}18)$$

For the plane wave, the electric field $\vec{E}$ and the magnetic field $\vec{H}$ are defined by

$$\vec{k} \times \vec{E} = \omega\mu\vec{H} \quad (1\text{-}19)$$

$$\vec{k} \times \vec{H} = -\omega\varepsilon\vec{E} \quad (1\text{-}20)$$

In the isotropic and homogeneous medium, the values of ε and μ are simultaneously positive. Therefore the electric field $\vec{E}$, magnetic field $\vec{H}$ and propagation vector $\vec{k}$ form right-handed medium (RHM), where the $\vec{S}$ and $\vec{k}$ have the same direction [13].

However if ε and μ are negative simultaneously, Eqs. (1-19) and (1-20) can be rewritten as:

$$\vec{k} \times \vec{E} = -\omega|\mu|\vec{H} \quad (1\text{-}21)$$

$$\vec{k} \times \vec{H} = \omega|\varepsilon|\vec{E} \quad (1\text{-}22)$$

In this case, the electric field $\vec{E}$, the magnetic field $\vec{H}$, and the propagation vector k form the left-hand medium (LHM) as depicted in Figure 1.5. In this medium, the Poynting vector $\vec{S}$ has the opposite direction to the propagation vector $\vec{k}$ so that it can support backward waves, i.e., the energy and wave fronts traveling opposite directions.

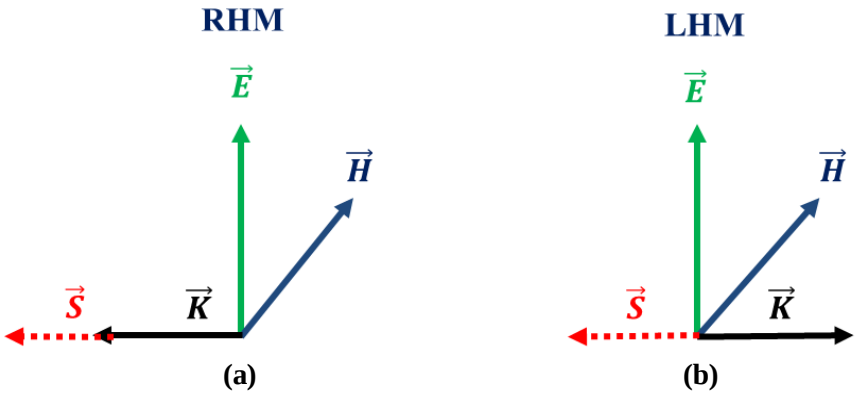

Figure 1.5 The vectors $\vec{E}$, $\vec{H}$ and $\vec{k}$ form (a) right hand media (b) left handed media.

1.3.2 Classification of Metamaterials

The electromagnetic properties of the materials, the dielectric permittivityε_r and the magnetic permeabilityμ_r determine how the electromagnetic waves propagate through a material. On the basis of its sign, the metamaterials can be classified into four groups, as it can be seen in Figure 1.6.

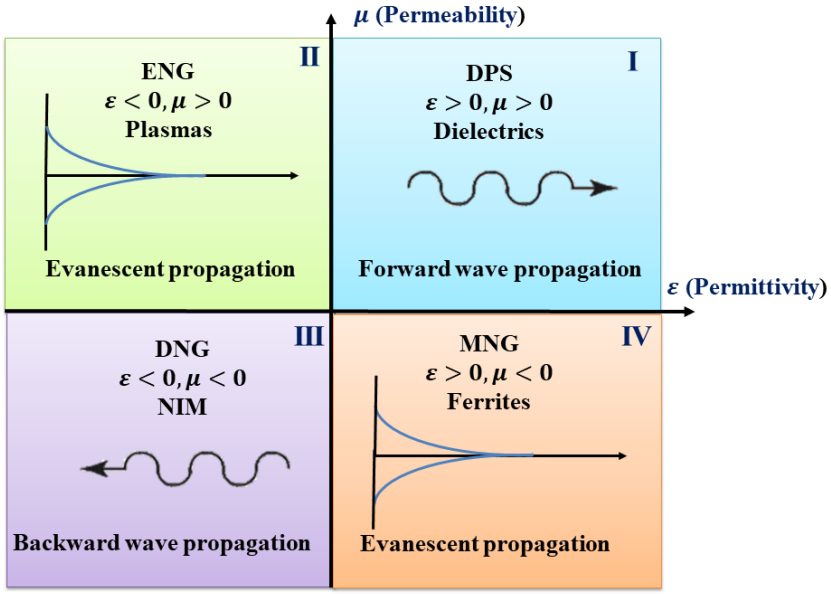

Figure 1.6 The classification of electromagnetic MTMs based on signs of the ε and μ.

1.3.2.1 Double Positive (DPS) Material

The materials which have both permittivity and permeability greater than zero (ε> 0, μ> 0) are called as double positive (DPS) materials. Most occurring media (e.g. dielectrics) fall under this designation.

1.3.2.2 Epsilon Negative (ENG) Metamaterial

If a material has permittivity less than zero and permeability greater than zero (ε< 0, μ> 0) it is called as epsilon negative (ENG) material. The ENG metamaterial uses the metallic mesh of thin wires, made of copper, aluminum ,silver or gold and they are arranged periodically (the period p and the radius of the wire *r*) as shown in Figure 1.7 .These parallel metal wires exhibit high-pass behavior for an incoming plane wave, whose electric field is parallel to the wires [14]. The

cylindrical array displays the negative permittivity below the cut off frequency as shown in Figure 1.7 (b), and total reflection is observed. This behavior is similar to the propagation of electromagnetic waves in the plasma medium.

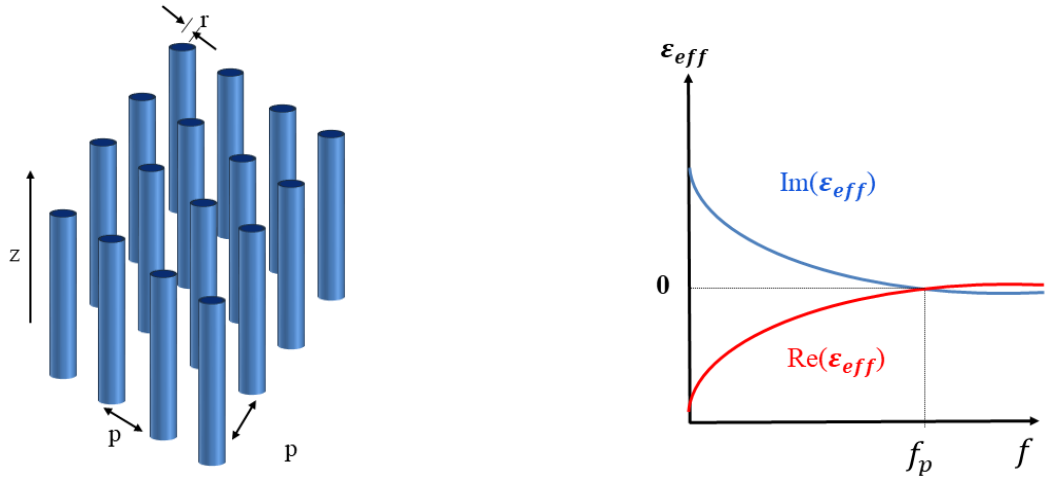

(a) **(b)**

Figure 1.7 An array of thin conducting wires **(a),** plots of the effective permittivity of an array of wires **(b)**.

1.3.2.3 Mu Negative (MNG) Metamaterial

If a material has permittivity greater than zero and permeability less than zero (ε> 0, μ< 0) it is called as mu negative (MNG) material. The most popular structure has been used is split ring resonators (SRRs) [14]. A unit cell of the SRR is composed of two concentric metallic rings (can be circle or square) and separated by a gap d. Each ring has a narrow slot, and they are spaced 180 degree apart on each side (see Figure 1.8(a)). The gap between inner and outer ring acts as a capacitor, while the rings themselves act as an inductors. Therefore, the combination of the two rings acts as an LC resonance circuit [14]. The metamaterial formed by the SRR array exhibits a negative permeability in a certain frequency region above the magnetic resonance f_{mp} as shown in Figure 1.8 (b) [15].

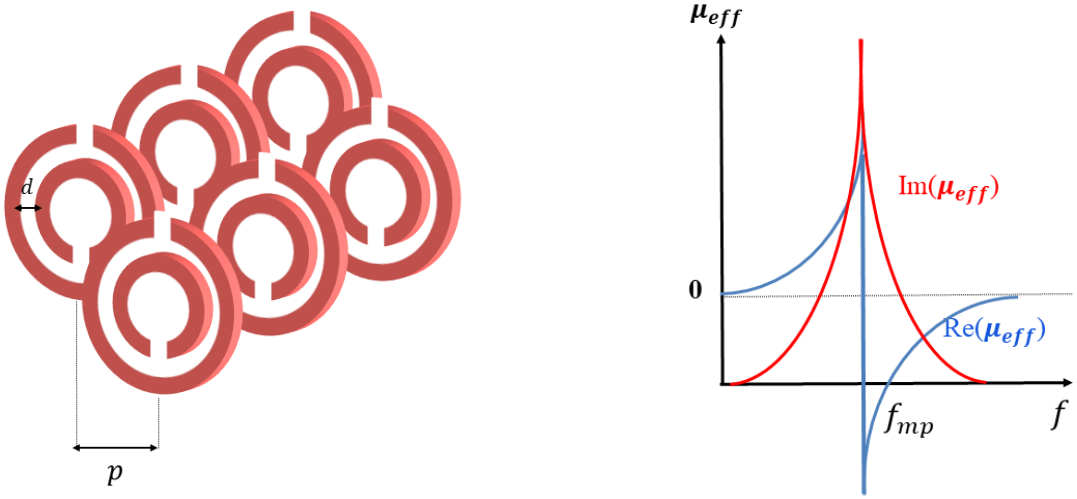

(a) **(b)**

Figure 1.8 An array of SRRs **(a)**, the effective permeability of SRR array **(b).**

1.3.2.4 Double Negative (DNG) Metamaterial

If a material has permittivity and permeability less than zero ($\varepsilon < 0, \mu < 0$) it is termed as double negative (DNG) material. This material is also known as the negative refractive index material (NIM). The properties of the metamaterials DNG were first achieved by combining the thin wire-based ENG structure with SRR-based MNG structure as shown in Figure 1.9 [14]. This combination satisfies the requirement of $\varepsilon < 0$ from a wire/rodded medium (as an artificial dielectric) and $\mu < 0$ from a split ring resonator (SRR).

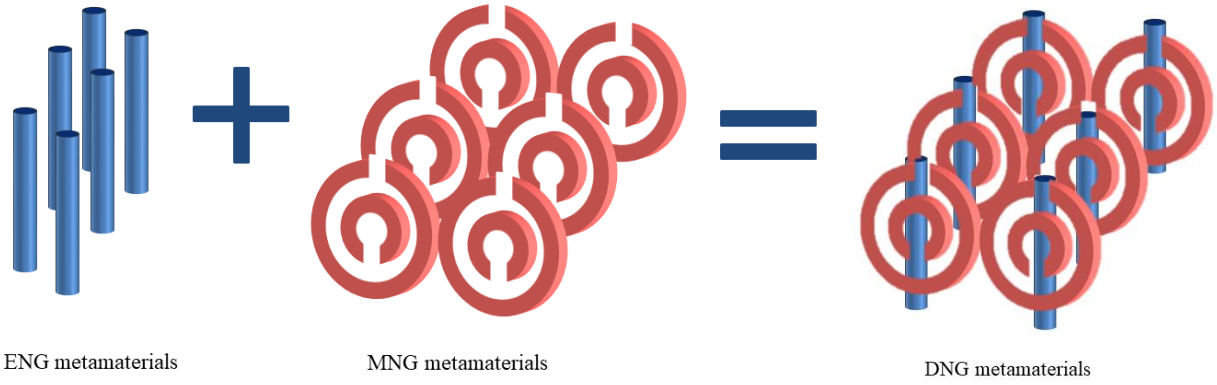

Figure 1.9 Combination of thin wires and SRR to form DNG metamaterials.

The first structure was constructed from the combination of planar SRRs etched on a thin dielectric layer and metallic rods (Figure 1.10a). In addition, to take advantage of the two sides of the dielectric layers, two-dimensional metamaterials have been designed by engraving the SRR on one side of the dielectric layer and planar strips on the other (Figure 1.10b)[14].

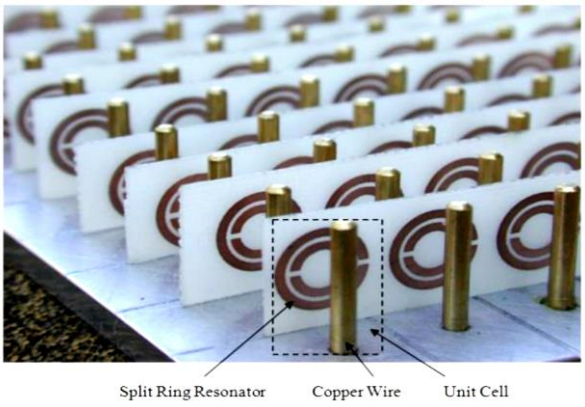

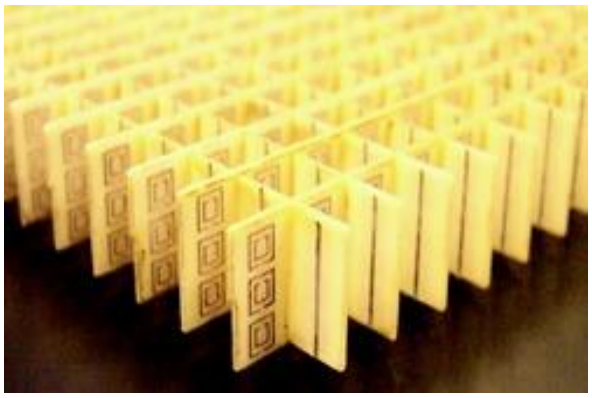

(a) **(b)**

Figure 1.10 Examples of realizations of DNG metamaterials **(a)** and **(b)**.

1.3.3 Metamaterials Types

1.3.3.1 Electromagnetic Band Gap (EBG) Metamaterials

EBG structures are defined as artificial periodic structures that avert or assist the propagation of electromagnetic waves in a specified band of frequencies for all incident angles and all polarization states [16]. EBG structures are always used as a part of microwave devices in order to improve the performance of devices especially to improve the radiation/gain patterns and to decrease the noise /losses in transmissions. EBG structures are also known as high impedance surface due to their ability to suppress the surface wave at certain operational frequencies. On the basis of dimensions, as shown in Figure 1.11 ,EBG structures are categorized as one dimensional

(1-D), two dimensional (2-D), and three dimensional (3-D) periodic structures that satisfies Bragg's conditions, i.e., inter-cell separation (period) is close to half guided wavelength (λg/2).They are capable of forbidding electromagnetic propagation in either all or selected directions[16].

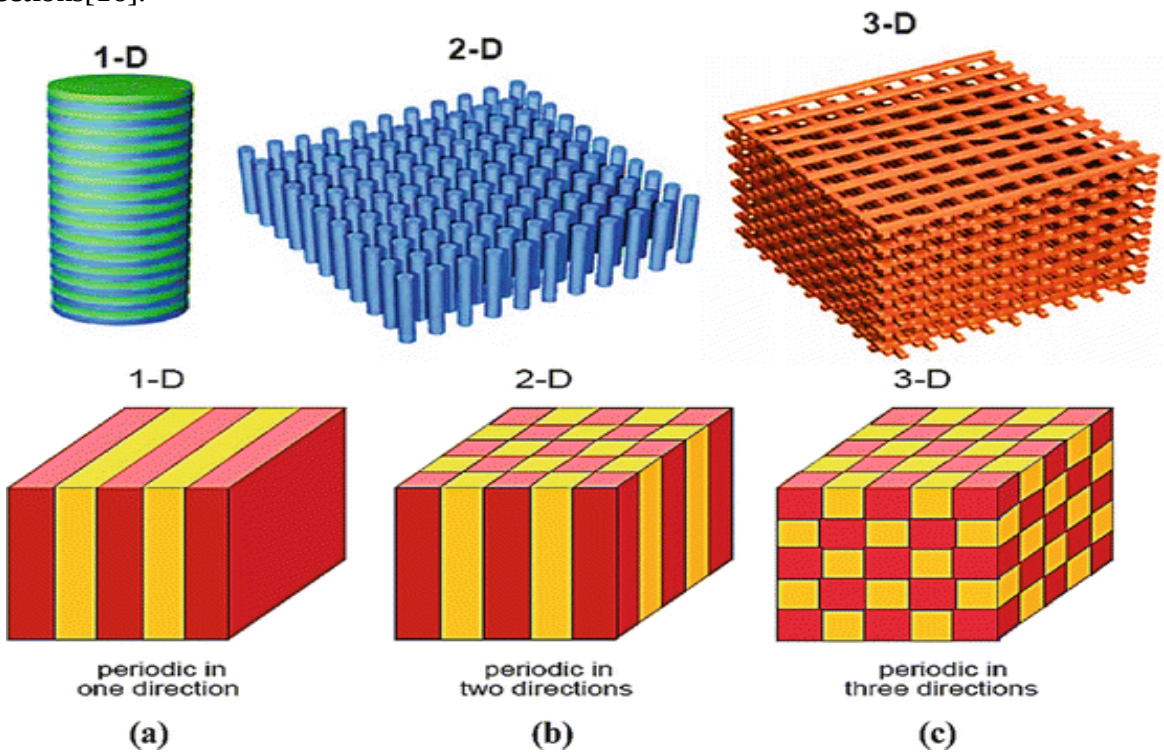

Figure 1.11 Types of electromagnetic bandgaps based on geometrical shapes,
(a)1D **(b)** 2D **(c)** 3D.

1.3.3.2 Frequency Selective Surface (FSS) Based Metamaterials

Traditionally, frequency selective surfaces have been defined as "a periodic array of identical elements arranged as a one or two dimensional array of metallic structures "[17]. While this definition is extremely broad, all the possible combinations of "periodic arrays of identical elements" can be categorized into two distinct subclasses, dipole arrays and slot arrays [17]. Examples of these two subclasses can be seen in Figure 1.12. Shown within this figure are two periodic arrays of metallic elements and slots on a dielectric substrate.

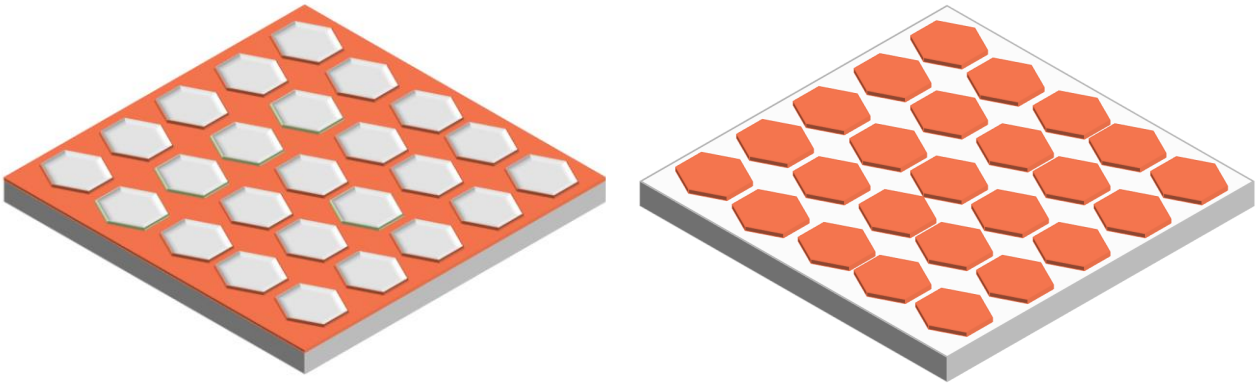

(a) (b)

Figure 1.12 Two examples of metallic FSSs,
(a) Slot array on a dielectric sheet (**b)** Dipole array on a dielectric sheet.

a. **Dipole Subclass of FSS**

It lays a great variety of geometries that further diversifies the type of shapes these devices can have. Through all the diversity in geometry the physical phenomenon on how they operate is the same. When an incident plane wave hits the dipole array FSS, it excites the metallic elements with electric currents causing the electrons within the elements to start oscillating. This electron oscillation in turn starts producing its own radiating electric fields as a array of tiny radiating antennas. It is the interference of this element radiation with the incident plane wave that produces the frequency selectivity response in these devices [18].

b. Slot array subclass of FSS

It is the same as the dipole array except for one key difference. Instead of inducing oscillating electric currents on metallic elements, the incident plane wave induces oscillating magnetic currents on the metallic surface [18]. These oscillating magnetic currents in turn cause the surface to start radiating its own field. Like the dipole array it is the interference of this surface radiation with the incident plane wave that produces the frequency selectivity response in these devices [18].

There is a very interesting relationship between the dipole and slot array FSSs. In most cases the dipole array acts as a band-stop filter while its complimentary slot array as a band-pass. This is known as Babinet's principal [18].

Babinet's Principle is actually the principle used in optics. According to its definition, "When the field behind a screen with an opening is added to the field of a complementary structure, the sum is equal to the field when there is no screen" [19].

1.3.3.3 Artificial Magnetic Conductor (AMC)

An AMC and also is known as High Impedance Surface (HIS) is a kind of metamaterial which has the property of a Perfect Magnetic Conductor (PMC). A useful PMC characteristic that mimicked by AMC is the ability to provide zero-degree reflection phases at its resonant frequency and the range of frequencies where the reflection phase is $-90°$ to $+90°$ is usually accepted as the AMC region and thus defined as its bandwidth [20].

Figure 1.13 illustrates a PEC and an AMC very close to a radiator such as an antenna. When an antenna is backed by a PEC plane with spacing less than $\lambda/4$, its $-180°$ reflection phase causes destructive interference to the forward propagating radiation and yielding poor return loss and in turn low total efficiency [20].

In contrast, if the antenna is backed by AMC plane with very small spacing, the in phase reflection causes constructive interference to the forward propagating radiation. Consequently, the radiation will be enhanced, low profile structure becomes feasible and good return loss can be achieved.

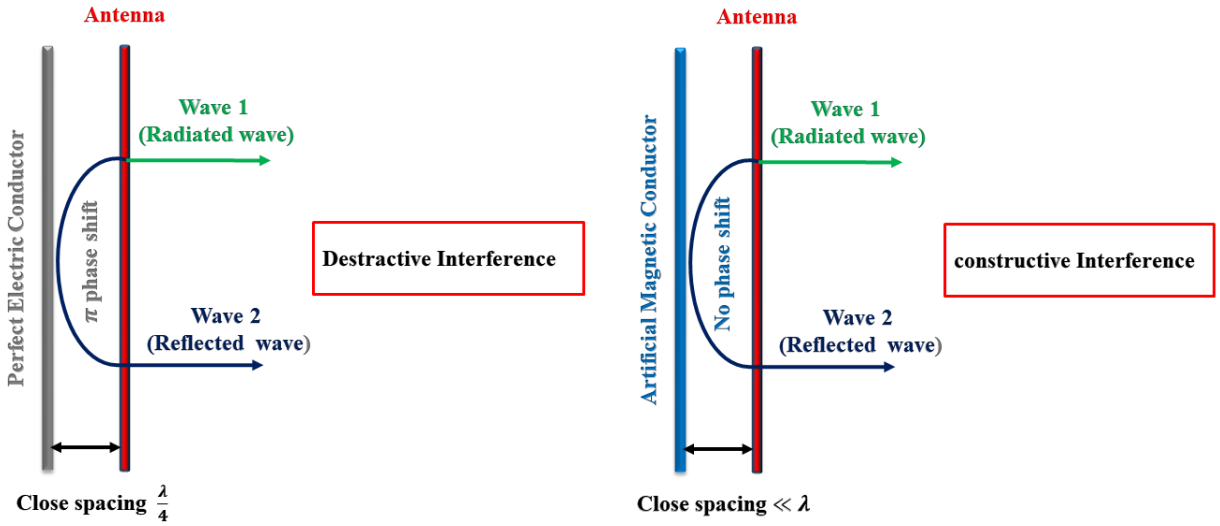

Figure 1.13 A radiator lying flat against, **(a)** PEC **(b)** a Metamaterial AMC.

1.4 Conclusion

This chapter has been divided into two main parts. In the first part a short overview of a microstrip antenna including standard definitions and fundamental antenna parameters and characteristics have been presented. In the second part the concept of metamaterial based on its properties, classification and types has been briefly introduced. For more detailed understanding on the behavior of microstrip antenna, the design and analysis of a novel dual band CPW monopole antenna will be discussed in the next chapter.

CHAPTER 02

Design of Dual Band Microstrip Antenna

CHAPTER 02: Design of Dual Band Microstrip Antenna

2.1 Introduction

Some of the most common uses of an antenna are its dual band design, which allows the same antenna to radiate in two different frequency bands. Many applications in recent wireless communication systems, such as GPS and GSM services operating on two different frequency bands, have become necessary. This chapter attempts to design and analyze a dual band monopole antenna to operate at 2.45 GHz and 5.20 GHz with coplanar line module using CST simulator software.

2.2 Design of Dual-Band Microstrip Antenna

For the 2.45/5.2 GHz dual-band WLAN application, a triangular ring antenna with coplanar feed line (CPW) using the FR-4 substrate with relative dielectric permittivity $\varepsilon_r = 4.3$, loss tangent $tan\delta = 0.025$ and thickness $h = 1.62\ mm$ is designed as shown in Figure 2.1.

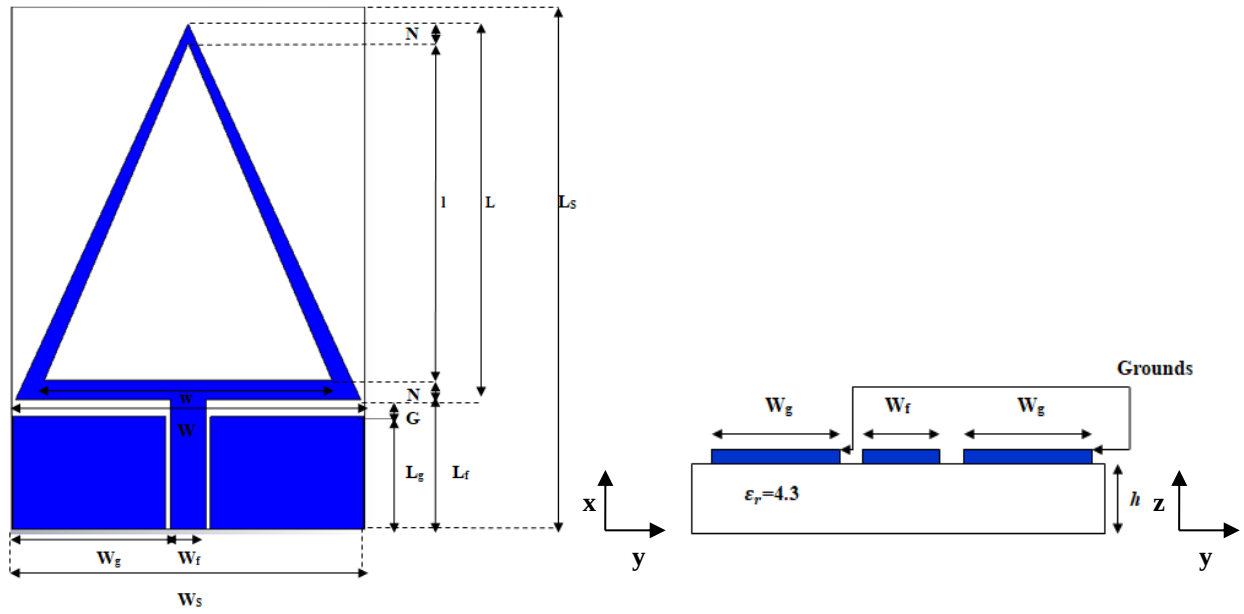

(a) (b)

Figure 2.1 Geometry and dimensions of CPW-fed triangular ring microstrip antenna, (a) Top view (b) Side view.

Table 2.1 displays the optimized parameters of the antenna such that the width of the feed line and the gap between the feed and the rectangular ground have been chosen so that the line impedance is 50 Ω as shown in Appendix A.

Table 2.1 The dimensions of the CPW triangular ring microstrip antenna.

Parameters	W_S	L_S	W_g	L_g	W	L	l	w	L_f	W_f	N	G
Value (mm)	30.136	45.17	13.12	9.72	29.53	32.5	29.1	24.5853	11.17	3.08	1.7	1.45

2.3 Simulation and Results

Waveguide ports represent a special kind of boundary condition of the calculation domain, enabling the stimulation as well as the absorption of energy [21]. Very low reflections can be achieved when the waveguide mode patterns in the port match perfectly with the mode patterns from the waveguides inside the structure where the energy in the EM fields around the line are

captured so that the port impedance can be calculated correctly. The waveguide ports depend a bit on the type of the transmission line [21]. For example, the port assignment for empty waveguides or coaxial waveguides is very simple, just it is important to make sure that the port covers the entire cross-section of wave guides. However in case of microstrip line or coplanar line is relatively complex from an electromagnetic point of view. Therefore some things need to be considered when defining ports for this type of structure [21].

The coplanar line is a frequently used transmission line for high frequency devices .The waveguide is either called ungrounded coplanar line or grounded coplanar line depending on whether the substrate is backed by a metallic shielding or not [21].

The size of the port is a very important consideration, it should be chosen large enough to enclose the significant part of the coplanar line field and small enough that the higher order modes can not propagate, and only the fundamental modes should be considered at the port. To achieve those conditions the following picture shows the recommended size of the port used for the ungrounded coplanar [21].

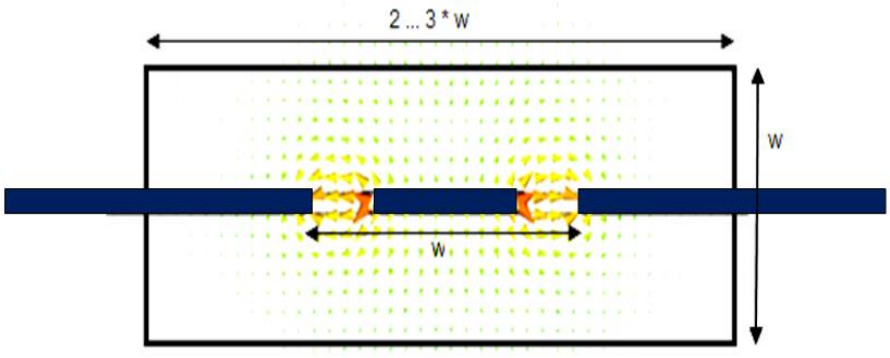

Figure 2.2 Ungrounded coplanar port size.

2.3.1 Parametric Study of the Proposed CPW Antenna

In order to understand the construction of the CPW antenna, a study was done on the effect of different parameters on its performance, noting that when one parameter is considered the others are kept constant.

a. Effect of the Triangular Slot

The patch antenna can be a full triangle or a slotted triangle as shown in shape (I) and shape (II) ,respectively. The effect of adding the slot on the input impedance of the triangular antenna is indicated in Figure 2.3. The input impedance of the full triangle shows that the structure resonates at 4.02 GHz with a real part of 314 Ω. When the triangle is slotted, it can be seen that the fundamental frequency is shifted to 2.45 GHz with a real part of 55.20 Ω and the second mode is appeared at 5.20 GHz with a real part of 55.14 Ω which are much closed to the line impedance (50 Ω) and this ensures a good matching with the feed line and a proper working of the antenna; note that another resonant frequency is occurred at 3.89 GHz with a real part of approximately 287.22 Ω, however the antenna cannot operate at this frequency since it is not matched to the line impedance (50 Ω). Consequently, it can be concluded that the slot was the responsible of the position of the two frequencies.

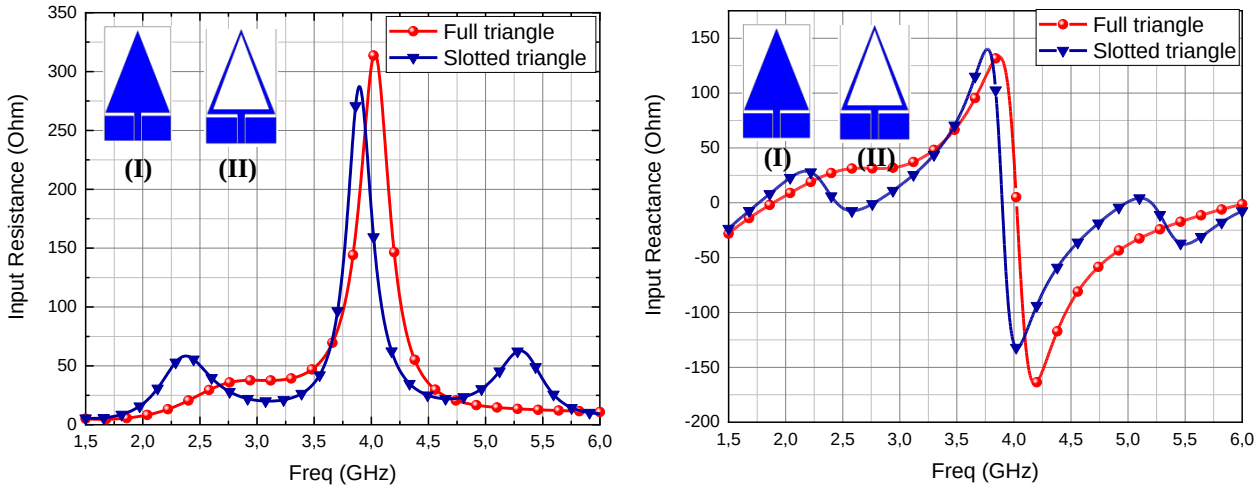

(a) **(b)**

Figure 2.3 Simulated input impedance for full triangle and slotted triangle structure, **(a)** Re (Z_{in}) **(b)** Im (Z_{in}).

b. Effect of The Height L and The Base W of Triangular Patch

The effect of varying L from 31.5mm to 33mm and W from 28.53mm to 30.03 mm on the input reflection coefficient of the CPW antenna is depicted in Figure 2.4.It can be seen that with an increase in L, both resonant frequencies are shifted to the lower frequency, while the input reflection coefficient is decreased as the value of L increases up to 32.5 mm. With further increase in L, the matching is reduced at both resonant frequencies. Whereas, the variation of W results in an insignificant change in the resonant frequencies but it affects the impedance matching of the first resonant frequency with.

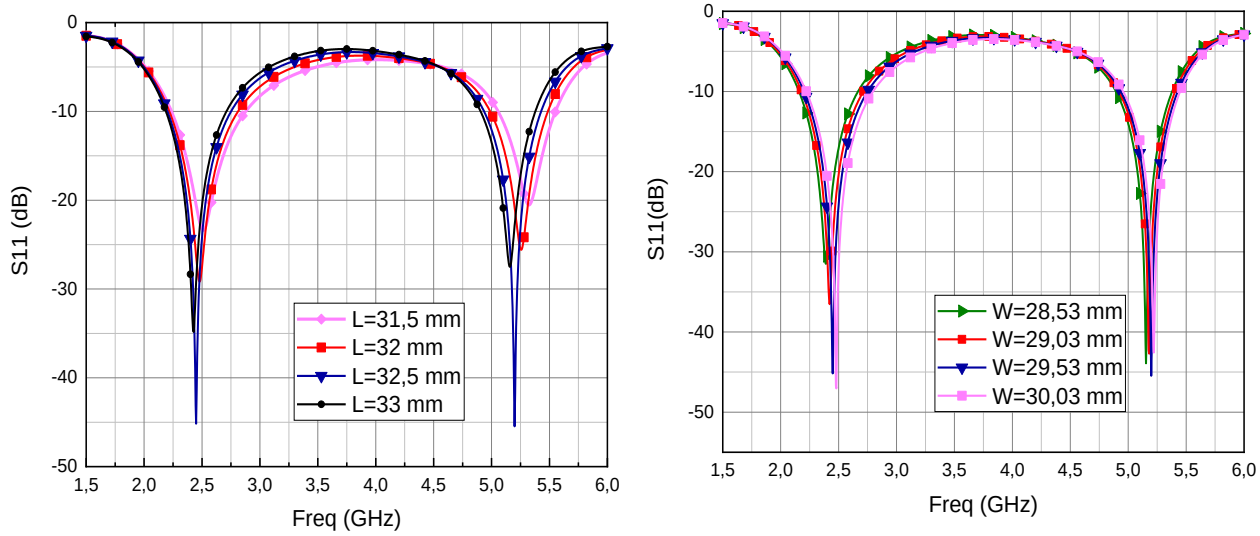

(a) **(b)**

Figure 2.4 Effect of varying the patch height and width on the input reflection coefficient , **(a)** effect of the patch height, L **(b)** effect of the patch width, W.

c. Effect of the Triangular Slot Height l and Base w

Figure 2.5 represents the effect of increasing l from 28.100 mm to 29.600 mm and w from 23.085 mm to26.085 mm.It is clear that the resonant frequencies remain unchanged with the variation of the height l. However; this variation affects the impedance matching of both frequencies. As indicated in figure 2.5a, the increase in l up to 29.100 mm results in the decrease in the S_{11} level. But as the value of l is further increase the matching is reduced at both resonant frequencies.

Figure 2.5b shows the effect of varying w. The resonant frequencies are highly affected by the parameter w.These frequencies are shifted down with the increase in w. The decrease in w, from 26.085*mm* to 24.585 *mm* at the first resonant frequency, results in the decrease of the level of S_{11}. But a further decrease in w raises the level of S_{11}. Also it is indicated that an increase in w results in the increase in the level of S_{11}at the second resonant frequency.

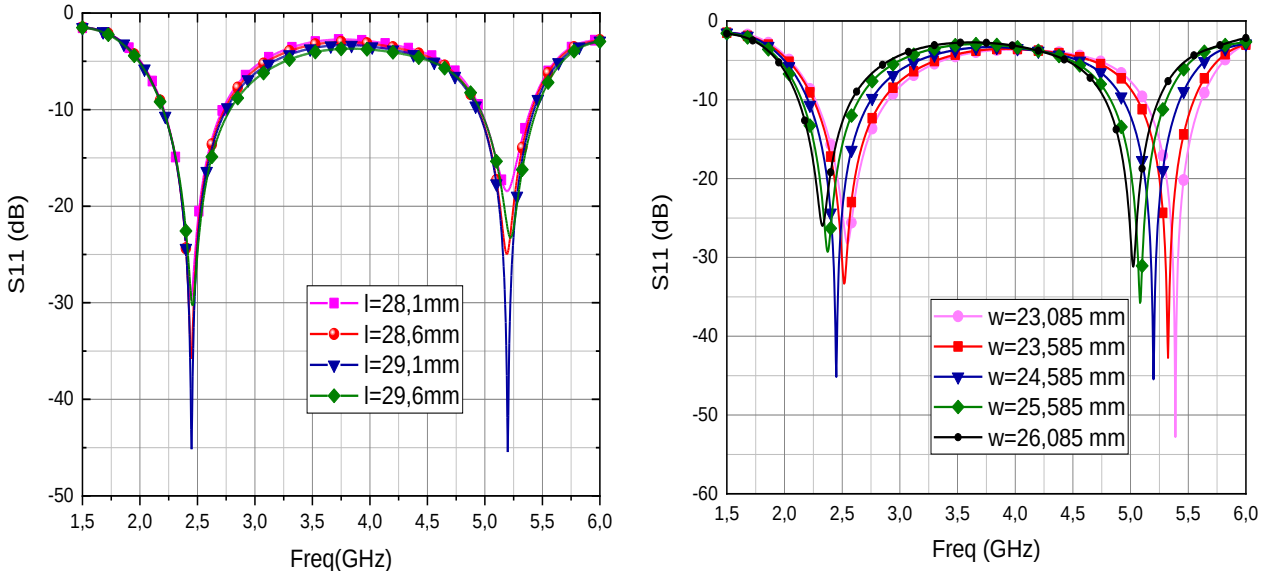

Figure 2.5 Effect of varying the slot height and width on the input reflection coefficient, (**a)** effect of the slot height, l **(b)** effect of the slot width, w.

d. Effect of the Gap width G and the Feed line Width W_f

The effect of changing G from 0.45*mm* to 2.45*mm* and W_f from 2.58 *mm* to 4.08 *mm* on the input reflection coefficient of the CPW antenna is shown in Figure 2.6.It can be observed that with an increase in G, the second resonant frequency is moved toward the higher frequency, while the input reflection coefficient at both resonant frequencies is reduced until G reaches 1.45mm. Beyond this value the S_{11} raises. The parameter W_f only affects the impedance matching without the resonant frequency values.

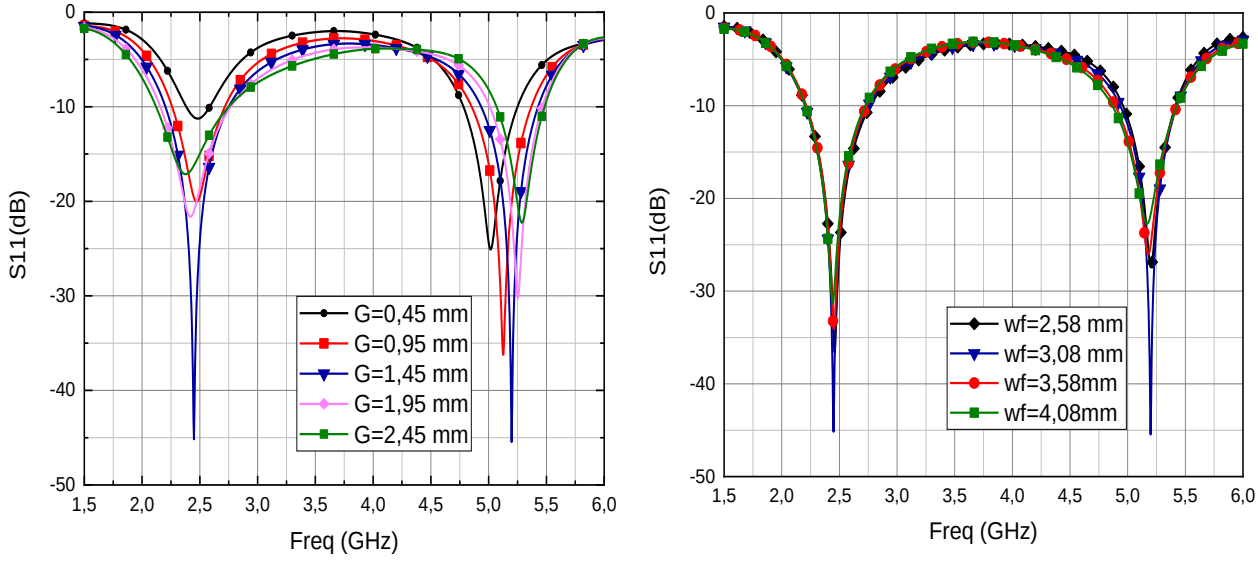

Figure 2.6 Effect of varying the gap between the patch and the ground and feed-line on the input reflection coefficient, **(a)**effect of the gap, G **(b)** effect of the feed line width, W_f.

Remark: Based on the above parametric analysis, the CPW antenna can be adjusted to the suitable design by proper choice of the parameter values as shown in Table 2.1. The final input reflection coefficient versus frequency is depicted in Figure 2.7.It can be seen that the antenna resonant frequencies are adjusted to the two distinct frequency bands centered at 2.449 and 5.199 GHz with a minimum reflection coefficient of-45.17 dB and -45.40 dB respectively. A-10 dB impedance bandwidths from 2.2 GHz to 2.75 GHz and from 4.93 GHz to 5.42 GHz are obtained around the first and the second resonant frequencies, respectively. The antenna covers WLAN standard$(2.4\ GHz, 5.2\ GHz)$ as wanted.

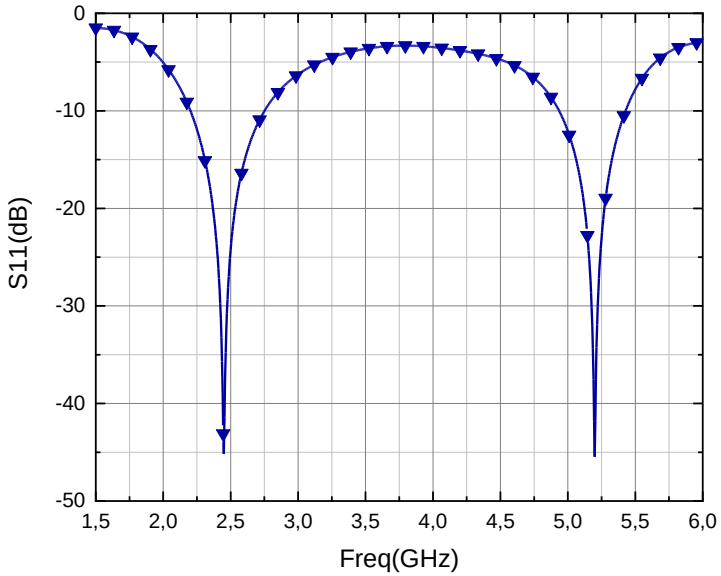

Figure 2.7 Simulated input reflection coefficient of the dual band CPW antenna.

2.3.2 Voltage Standing Wave Ratio

Figure 2.8 represents the CPW antenna VSWR. It is observed that the VSWR is one at both resonant frequencies, which means that no power is reflected from the antenna and there are no standing waves along the transmission line. So, at these two resonant frequencies the transmission line is well matched to the antenna.

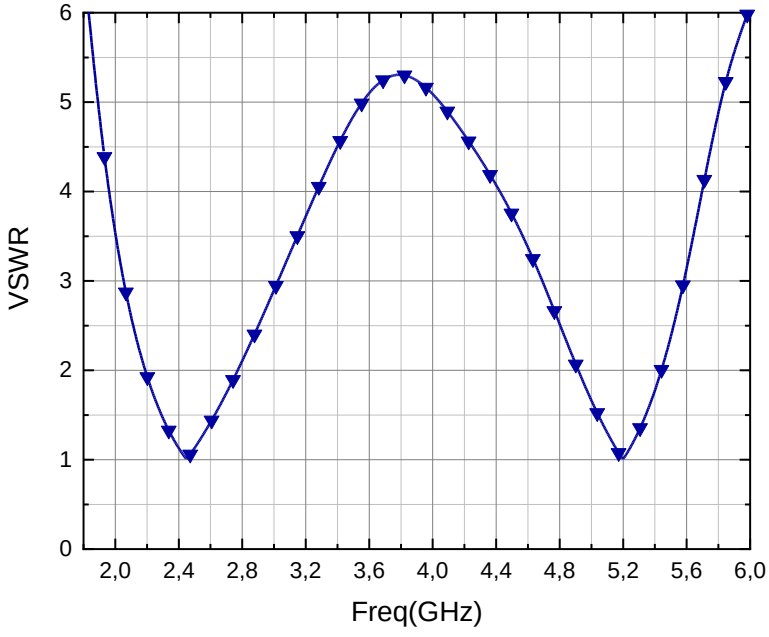

Figure 2.8 Simulated input VSWR of the dual band CPW antenna.

2.3.3 Current Distribution

The distribution of surface current is a significant parameter to be considered , it indicates how the current travels through the patch after feeding the antenna which informs about the radiation pattern.

Figure 2.9 shows the simulated current distribution of the CPW antenna at 2.45 GHz and 5.2GHz.It can be seen that many maxima appear at the higher frequency compared with the lower frequency since the antenna operates at the fundamental mode at the first frequency and higher order modes at the higher frequency with the lower wavelength. Also, this figure reveals about the parts of the antenna which are responsible on the radiation (parts that fixe the resonant frequency).

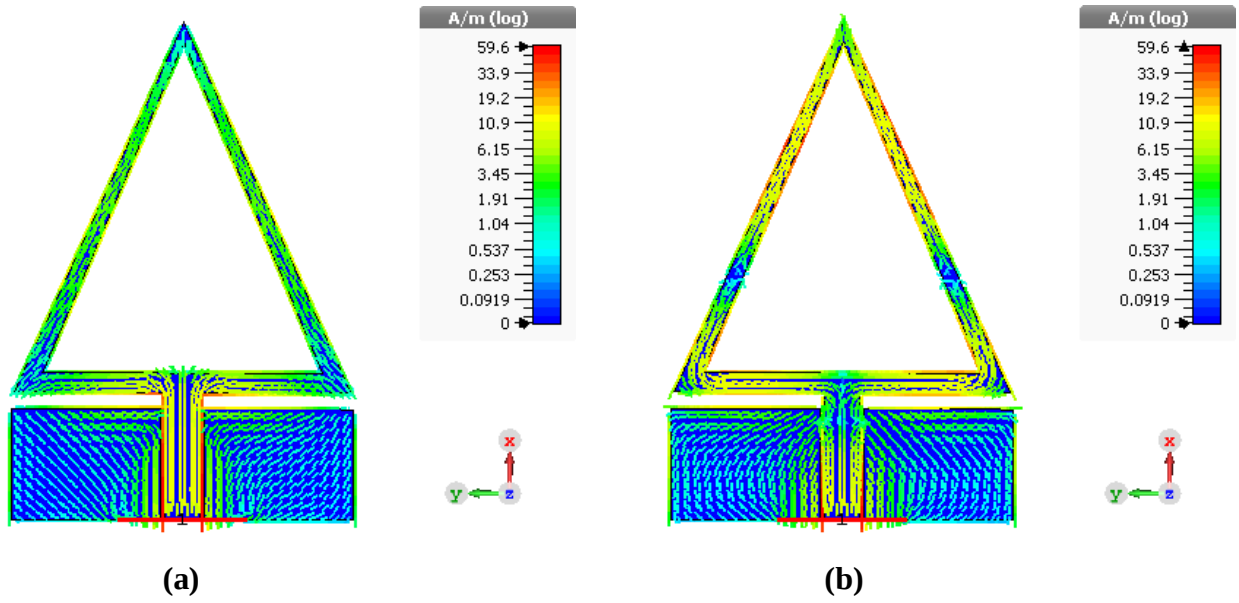

(a) **(b)**

Figure 2.9 The current distribution of the CPW antenna at **(a)** 2.45GHz, **(b)** 5.20 GHz.

2.3.4 Radiation Pattern

The simulated 2 D representation of the far field radiation patterns at 2.45 GHz and 5.2 GHz are shown in Figures 2.10 and 2.11 respectively. To study the polarization purity, both co-polar and cross-polar components of the radiated field are drawn in the main planes, E-plane and H-plane in the same figures. Since the feed line is on the x-axis, the antenna is x-polarized. The corresponding E_{co} and E_{cross} are expressed as

$$\begin{bmatrix} E_{co} \\ E_{cross} \end{bmatrix} = \begin{bmatrix} +cos\varphi & -sin\varphi \\ +sin\varphi & +cos\varphi \end{bmatrix} \begin{bmatrix} E_{\theta} \\ E_{\varphi} \end{bmatrix}$$

For $\varphi = 0°$ (E-plane) : $\begin{Bmatrix} E_{co} = E_{\theta} \\ E_{cross} = E_{\varphi} \end{Bmatrix}$ For $\varphi = 90°$ (H-plane) : $\begin{Bmatrix} E_{co} = -E_{\varphi} \\ E_{cross} = E_{\theta} \end{Bmatrix}$

Figure 2.10 shows that the antenna exhibits a broadside omnidirectional radiation at frequency 2.45 GHz. For the E-plane, the co-polar realized gain is 2.27 dBi with a beamwidth of about 82.1°, whereas the cross-polar realized gain is $-106.27dBi$ lower than the co-polar. The co-polar realized gain for the H-plane is 2.25 dBi, while the cross-polar is -33.65 dBi lower than the co-polar.

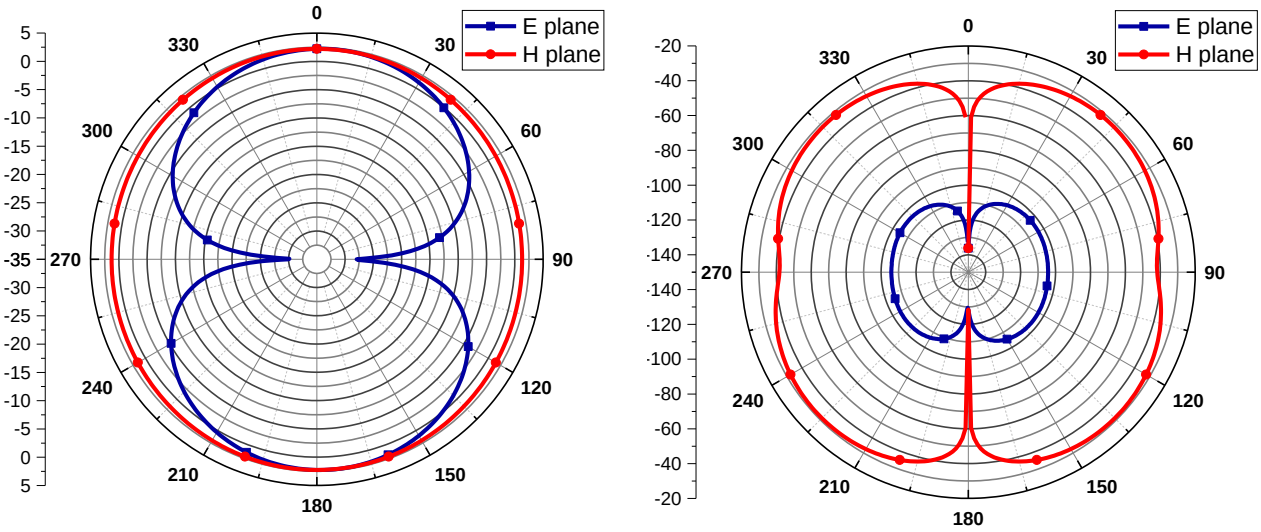

(a) **(b)**

Figure 2.10 Simulated radiation patterns of the proposed Antenna at 2.45 GHz, (a) Co-polar components (b) Cross-polar components.

Figure 2.11 indicates that at the frequency 5.2 GHz, the radiation pattern of the antenna is bidirectional and pinched around $\theta = 0°$in the E-plane as compared the radiation pattern at the 2.45 GHz, indicating that the antenna operates in the higher order mode. For the E-plane, the co-polar realized gain is 2.22 dBi with a beamwidth of about 47.6° with respect to 142° main lobe direction which is smaller than the beamwidth of the radiation pattern at the first resonant frequency due to pinches. The cross-polar pattern has a realized gain of $-100.82\ dBi$ lower than the co-polar.For the H-plane, the co-polar pattern is less pinched around $\theta = 0°$ as compared to the co-polar component and its realized gain is $0.44\ dBi$, while the cross-polar realized gain is about$-21\ dBi$ lower than the co-polar.

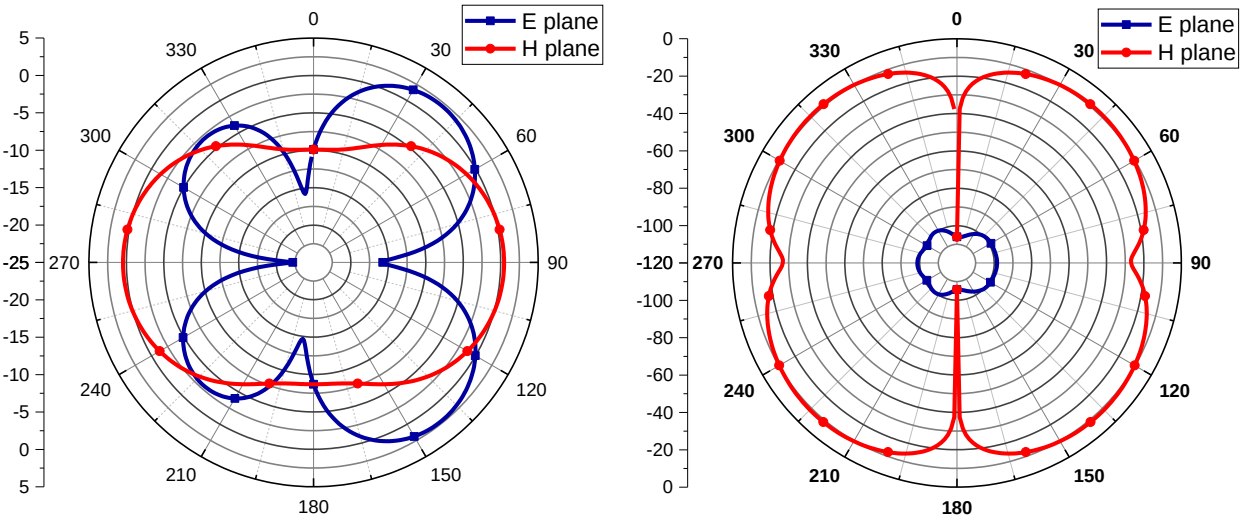

(a) **(b)**

Figure 2.11 Simulated radiation patterns of the proposed Antenna at 5.20 GHz, (a)Co-polar components(b)Cross-polar components.

Figure 2.12 shows the simulated 3D radiation patterns of the CPW antenna at 2.45GHz and 5.20 GHz. The radiation pattern looks like a doughnut, similar to a dipole pattern at the lower band resonant frequency with a maximum directivity$D = 2.48\ dBi$.While at the higher band resonant frequency, the pattern looks like a slightly pinched doughnut with maximum

directivity $D = 3.11\ dBi$.This increasing in directivity is due to the fact that directivity is weak for wavelengths that are much larger than the physical size of the antenna but it increases for short wavelengths. That is exactly what is observed; the radiation field is omnidirectional for wavelengths much greater than the physical size (i.e., the lower resonant frequency); in comparison, the radiation field is bidirectional in the short wavelength (i.e., the higher resonant frequency).

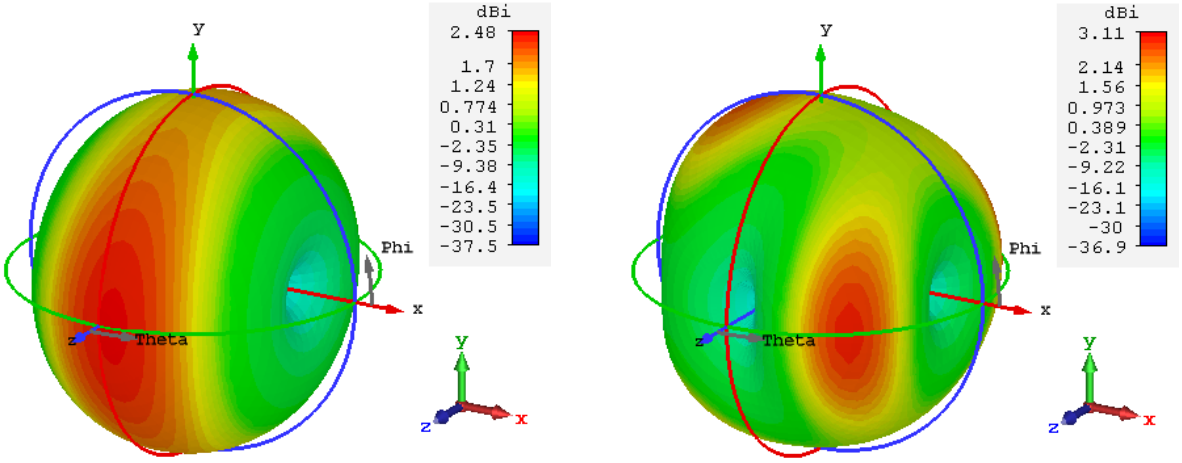

(a) (b)

Figure 2.12 Simulated 3D radiation patterns of the proposed Antenna.
(a) pattern at 2.45GHz **(b)** pattern at 5.20 GHz.

2.3.5 Antenna Efficiency

The antenna efficiency is one of the most important parameters to study in the antenna since it takes into account the mismatch loss, dielectric loss and conductor loss. The plots of different types of efficiency versus frequency are represented in Figure 2.13.It can be seen that the reflection efficiency achieves the unity at the low and high band resonant frequencies due to the good matching. The radiation efficiencies are about 0.96 at 2.45 GHz and 0.81 at 5.2 GHz, which are practically high. Therefore the total efficiency at the two resonant frequencies is high.

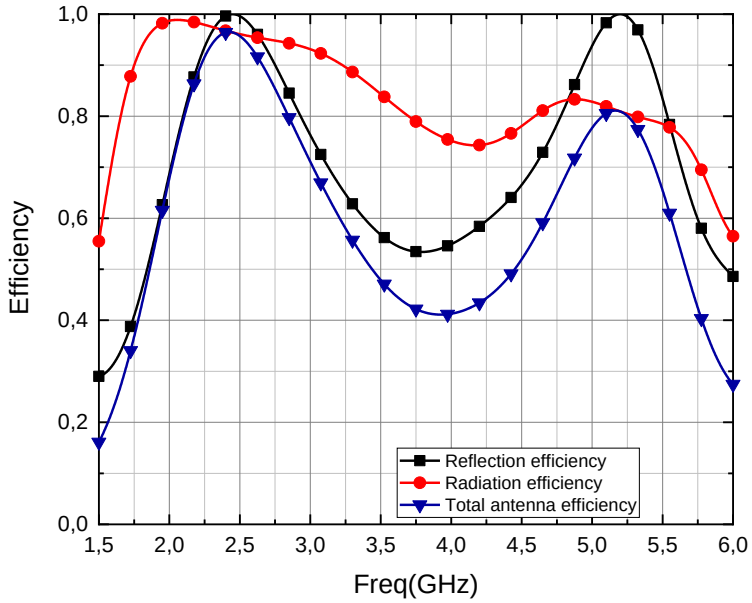

Figure 2.13 Antenna efficiency versus frequency of the CPW antenna.

2.3.6 Gain and Directivity

The simulated antenna gains and directivity versus frequency are shown in Figure 2.14.It can be observed that at both resonant frequencies, the IEEE gain and the realized gain are approximately the same. This means that the design has very low losses. Whereas the directivity is closed to the realized gain at the first resonant frequency more than the second resonant, due to the high radiation efficiency as it has been shown in figure 2.14.

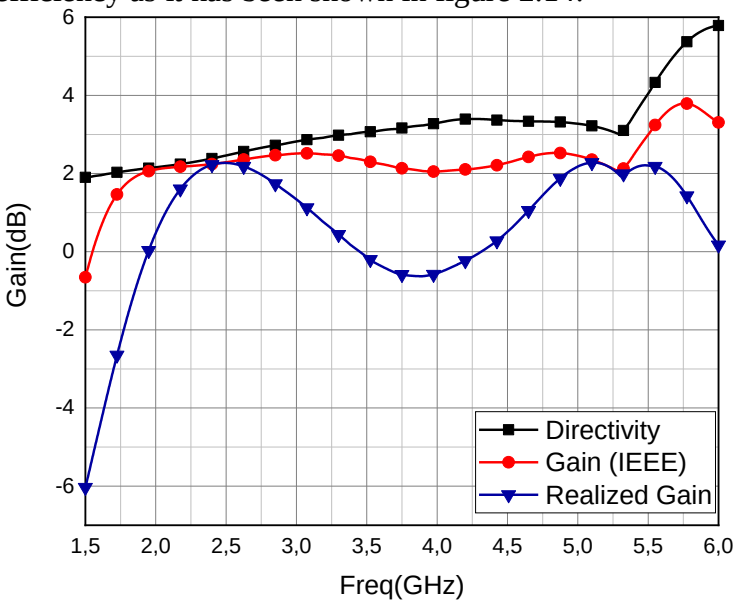

Figure 2.14 The simulated gains and directivity versus frequency of the CPW antenna.

2.4 Conclusion

In this chapter, a dual band CPW antenna has been designed and simulated using CST software. This antenna resonates at lower and higher frequency bands centered at $2.449GHz$ and $5.199\ GHz$ with input reflection coefficient of $-45.17dB$ and$-\ 45.40\ dB$ respectively, which are sufficient for matching. In addition, the antenna achieves a low realized gain of about $2.27\ dBi$ and $2.22\ dBi$, respectively at both resonant frequencies which can be considered as one of the drawbacks of microstrip antenna. To overcome this, a new artificial structure is used to enhance the gain will be discussed in the next chapter.

CHAPTER 03

Design of Dual Band AMC Unit Cell

CHAPTER 03: Design of Dual Band AMC Unit Cell

3.1 Introduction

Metamaterials have received much interest in the recent years because of their unique properties in controlling the propagation of electromagnetic waves, which allows them to solve certain antennas and microwave circuits problems. Artificial magnetic conductor AMC is a sub class of metamaterials that is designed to imitate the behavior of perfect magnetic conductor PMC that is not existed in nature. This type of metamaterial has attracted a lot of attention in recent years and it has been extensively used in antenna and microwave applications in order to improve the desired performances. The aim of this chapter is to provide further knowledge on the functioning of an AMC structure by designing and analyzing a novel dual band AMC unit cell to operate at 2.45 GHz and 5.20 GHz.

3.2 Design of Dual Band AMC Unit Cell

A novel structure of AMC unit cell is proposed to operate at 2.45 GHz and 5.2 GHz. The structure is printed on FR-4 substrate with thickness h = 1.62mm, relative permittivity $\varepsilon_r = 4.3$, and loss tangent $tan\delta = 0.017$. The other side of the substrate is a metallic ground plane, as depicted in Figure 3.1. The optimum dimensions of the AMC unit cell are shown in table 3.1.

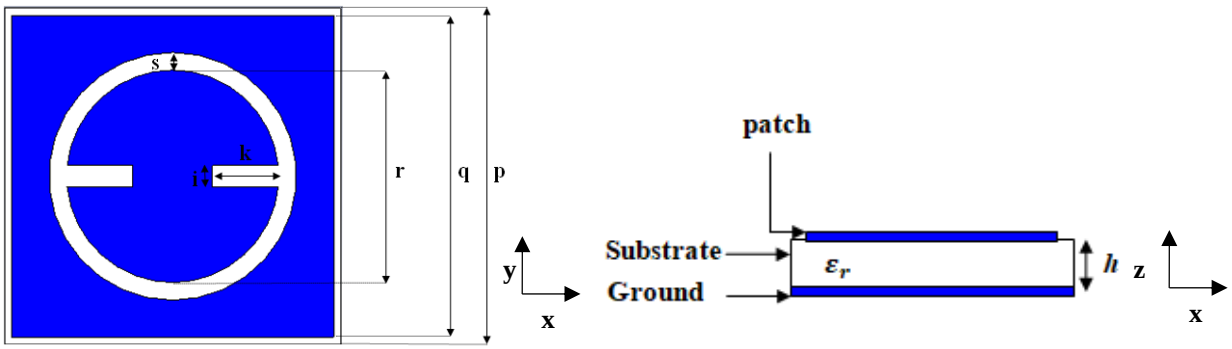

Figure 3.1 Geometry and dimensions of AMC unit cell,
(a) Top view (b) Side view.

Table 3.1 The dimensions of AMC unit cell.

Parameters	p	q	r	k	i	s
Value (mm)	19	18.2	12	3.75	1.2	1

3.3 Simulation and Results

The AMC structure is simulated using a waveguide setup to mimic the infinite array of AMC structure. The setup is designed in CST software using parallel E-plane and H-plane boundary condition and the system is excited by a waveguide port located at the top of the waveguide and de-embedded to the surface of the AMC structure [22], as shown in Figure 3.2. Note that the distance to the reference plane should be selected correctly to obtain the correct phase information of the s parameters [23].

Due to the boundary conditions given in the unit cell, the fundamental waveguide mode is TEM wave (uniform plane wave) that is normally incident on the structure, with its electric and magnetic fields along the *y* and *x* axis, respectively as it is shown in Figure 3.3.

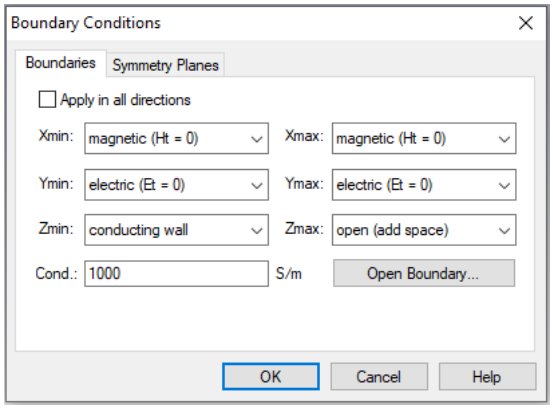

Figure 3.2 Boundary conditions setup of the proposed AMC unit cell.

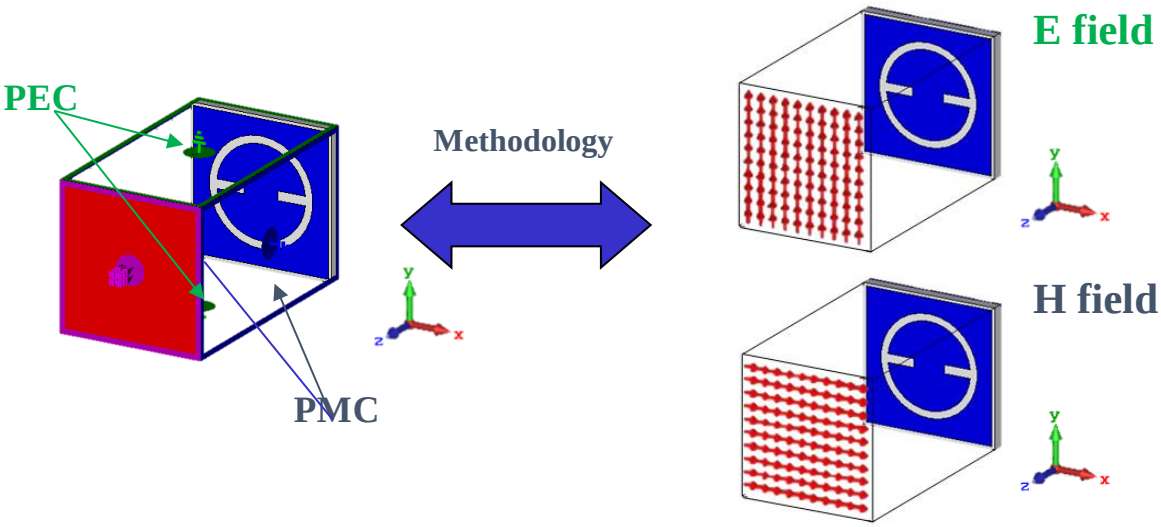

Figure 3.3 Boundary conditions methodology for the proposed AMC unit cell.

It is worth mentioning that the essential feature associated with the AMC surface is that it reflects the EM waves without any phase shift, unlike the PEC that reflects these waves with the 180° phase shift. Therefore the Incident and reflected EM waves are in phase over some AMC frequency bands. If this occurs, the AMC acts like a high impedance surface to the incident wave.

3.3.1 Parametric Study of the Proposed AMC Unit Cell

The resonance frequencies and the reflective bands of an AMC unit cell are determined by the unit-cell geometry, the dielectric permittivity, and the substrate thickness. Thus, for a specific substrate thickness and dielectric permittivity, the unit-cell design plays an important role in achieving dual-band behavior and in ensuring sufficient reflective band at each desired resonant frequency.

Figure 3.4 represents the reflection phase response at different stages of the dual band AMC unit cell. It can be observed that at the initial stage the unit cell resonates at 3.204 GHz with a large frequency band about 315 MHz. Then adding the circular slot in the square patch at the second stage shifts the resonant frequency to 2.46 GHz with reflective band about105 MHz. A higher resonant frequency band begins to appear after placing a circular metal

within the slot at the third stage with a slight change in the first band. Further inserting two rectangular slots in the circular patch at the last stage, the AMC unit cell exhibits dual band response and resonates at 2.484 GHz and 5.204 GHz.

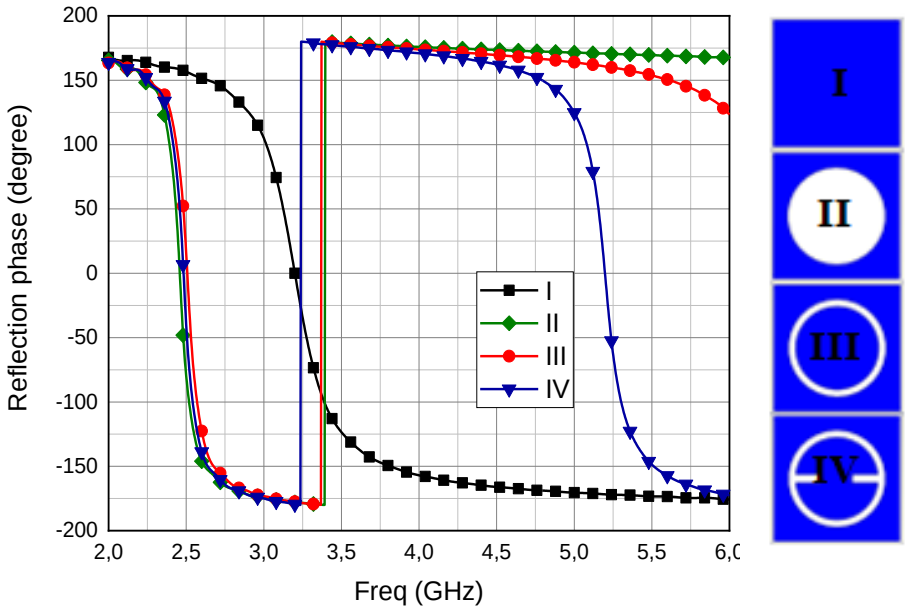

Figure 3.4 Reflection phase of the AMC unit cell at different stages.

To understand more about the construction of the dual band AMC unit cell, a comparative study was carried out on the effect of various parameters on the reflection phase. It should be noted that when one parameter is varied the others are kept constant.

a. Effect of the length q

The reflection phase versus frequency for different values of q from 16.7 mm to 18.2 mm is shown in Figure 3.5. It is clearly seen that the length q only affects the lower band. As the length q increases, the lower resonant frequency point is moved towards the lower frequency, because the gap between neighboring cells gets smaller by increasing q, as a result the capacity effect is increased which leads to the decrease of the resonant frequency [24].

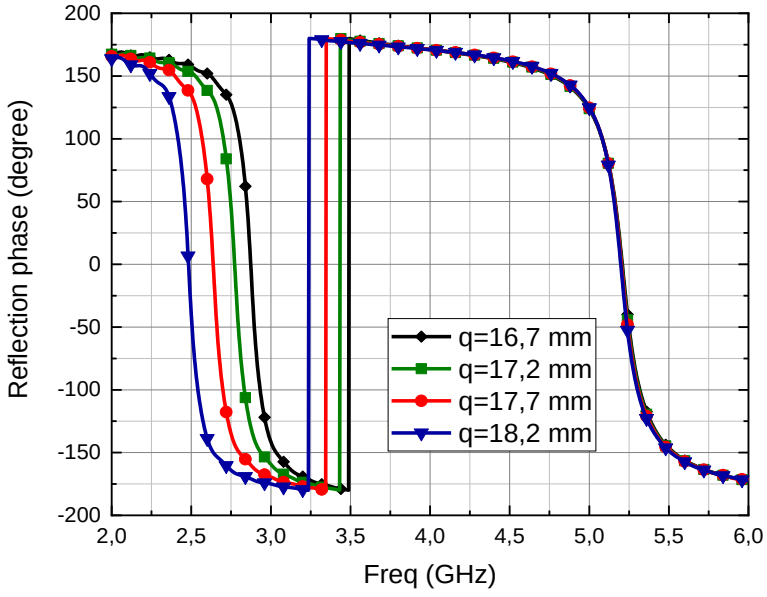

Figure 3.5 Effect of varying the length q on reflection phase.

b. Effect of the length r

The effect of varying r from 10 mm to 13 mm on the reflection phase of the AMC unit cell is depicted in Figure 3.6. It can be noticed that with an increase in the length r, both resonant frequency points are moved towards the lower frequencies, the lower band is decreased and the higher band is increased.

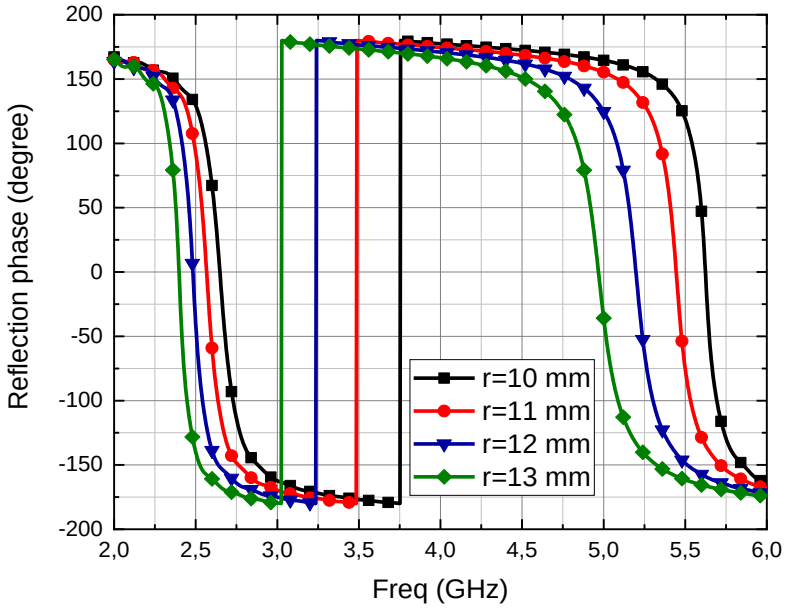

Figure 3.6 Effect of varying r on reflection phase.

c. Effect of the length k

Figure 3.7 represents the effect of increasing k from 2.75 mm to 4.25 mm on the reflection phase of the unit cell. It is clearly observed that the length k only affects the higher band. As the length k increases, the higher resonant frequency point is shifted towards the lower frequencies and its band is reduced.

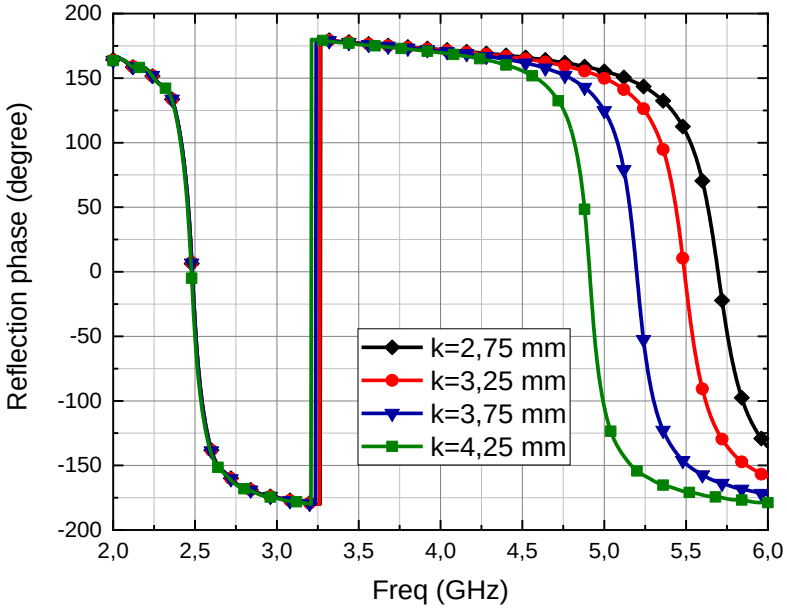

Figure 3.7 Effect of varying k on reflection phase.

d. Effect of the length s

The effect of changing s from 0.75 mm to 1.5 mm on the reflection phase of the unit cell is shown in figure 3.8. With an increase in s, the lower resonant frequency is moved towards the lower frequencies, whereas the higher resonant frequency is shifted towards the higher frequencies and both frequency bands are reduced.

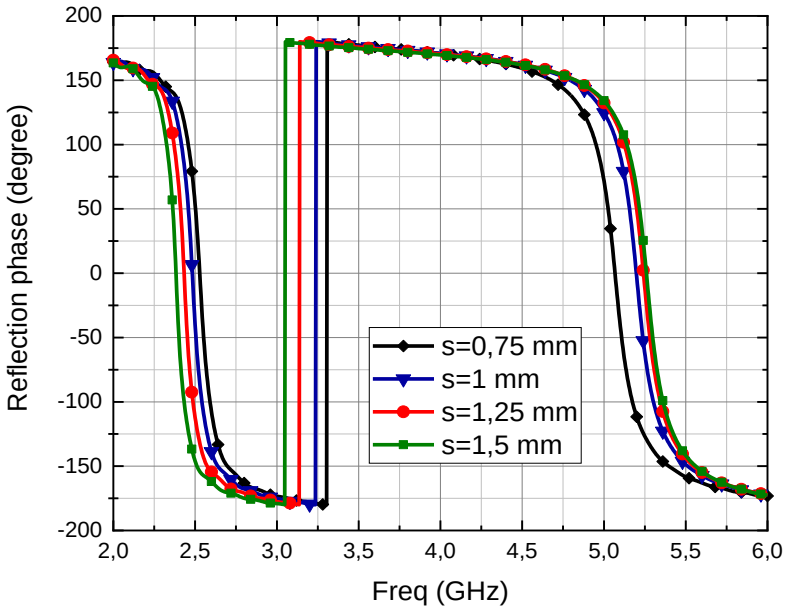

Figure 3.8 Effect of varying s on reflection phase.

e. Effect of the length i

Figure 3.9 shows the reflection phase curves when the length i varies from 0.7 mm to 1.45 mm. It can be seen that the lower band remains the same; however the higher band is shifted to the left as i is increased.

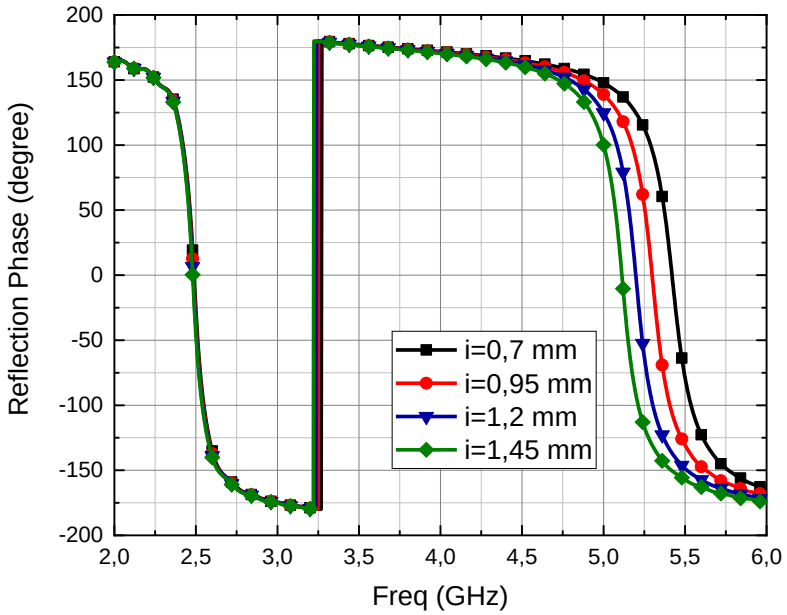

Figure 3.9 Effect of varying i on reflection phase.

Based on the above parametric analysis, the AMC unit cell can be adjusted to the suitable design using the optimizing values as shown in Table 3.1. The corresponding reflection phase versus frequency is depicted in Figure 3.10. It can be seen that the AMC operation bandwidth, which is defined in the range from -90° to 90° is narrow about 104 MHz in the lower frequency band centered at 2.484GHz, while the higher frequency band centered at 5.204 GHz is about 183 MHz. Outside these two bands, the unit cell acts as a PEC surface with $\pm\pi$ reflection phase.

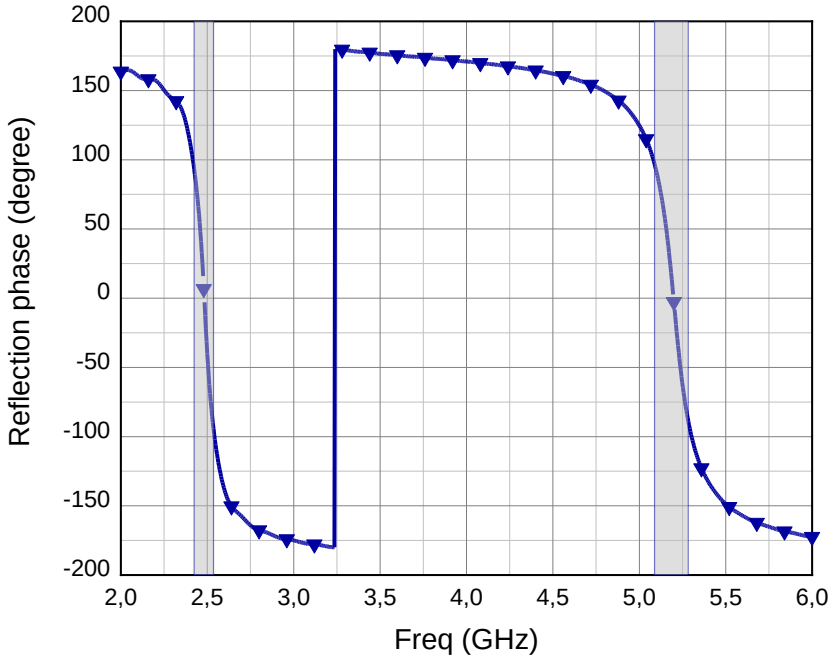

Figure 3.10 Reflection phase response for proposed AMC unit cell.

Remark: in case the incident wave is normal to the surface**,** the reflection phase of a surface with impedance Z_s is given by [25]

$$\varphi = arg\left(\frac{Z_s-\eta_0}{Z_s+\eta_0}\right) \tag{3-1}$$

Where φ is the reflection phase and η_0 is the intrinsic impedance of the free space. It implies that when Z_s is very high the reflection phase is zero, in contrast if Z_s is very low the reflection phase is $\pm 180°$. Moreover; if the phase reaches$\pm 90°$ implies that the surface impedance is equal in magnitude to the impedance of free space, those properties can be seen in Figure 3.11.

3.3.2 Surface Impedance

Unlike PEC, the AMC unit cell behaves as a high impedance surface. Figure 3.11 shows the general behavior of the surface impedance versus frequency for the proposed structure. It can be observed that compared to the impedance of free space, the surface impedance is extremely high in the narrow region close to both lower and higher resonant frequencies where it reaches 877.01 Ω and 900.73 Ω respectively. Below the resonance, the surface impedance shows an inductive behavior which supports the propagation of TM waves however above the resonance, it shows a capacitive behavior and TE waves are supported [26].

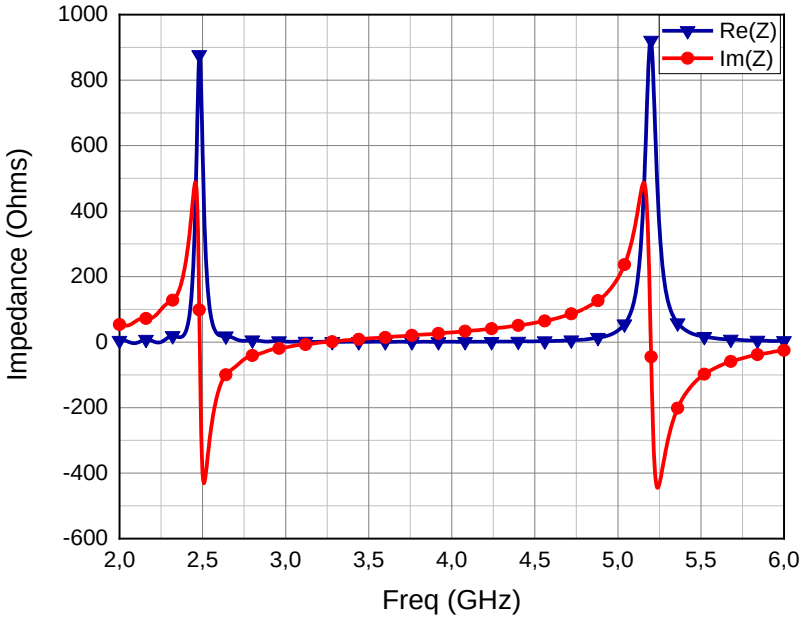

Figure 3.11 Surface impedance of the dual band AMC unit cell.

3.3.3 Current distribution

Figure 3.12 displays the simulated current distribution of the AMC unit cell at 2.45 GHz and 5.20 GHz. It is shown that the surface current at 2.45 GHz is distributed over the entire square patch, whereas the current at 5.20 GHz primary lies in the inner circular metal and it is extremely higher in the edges of both rectangular slots. It can be concluded that the inner circular patch with both rectangular slots has a decisive impact on the higher resonant frequency and this result is consistent with the one which is obtained from Figure 3.4.

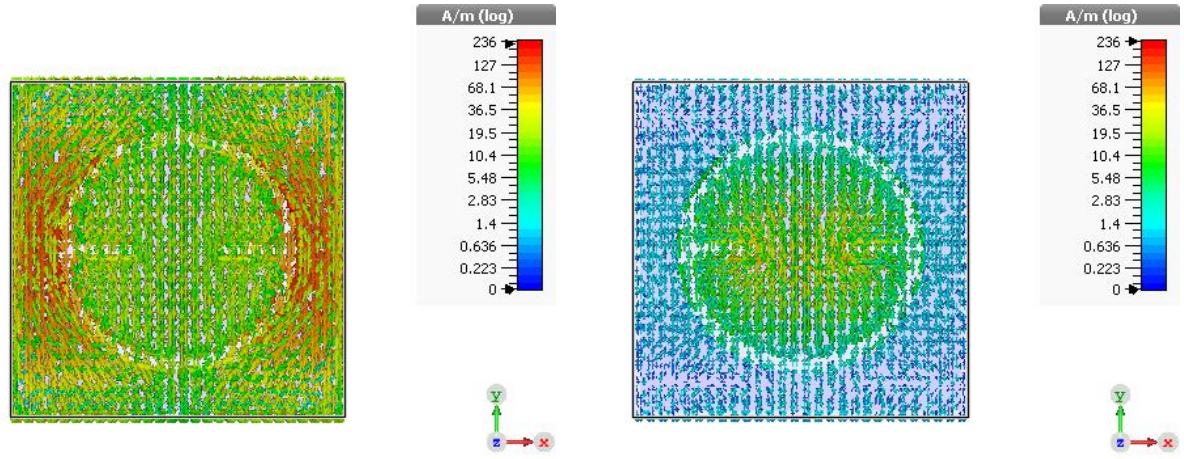

(a) **(b)**

Figure 3.12 Current distribution of the dual band AMC unit cell at,

(a) 2.45 GHz **(b)** 5.20 GHz.

3.3.4 Periodic structure

In order to obtain the limit dimension of the AMC surface, different arrays of unit cells have been simulated using the same boundary conditions; the corresponding reflection phases are shown in Figure 3.13. It can be seen that as we increase the number of the unit cells, the lower frequency band moves to the left due to the mutual interactions and coupling between the elements. When the AMC surface reaches the size of 7 by 7 arrays, the frequency 2.45 GHz gets

out from the AMC operating region which makes the 6 by 6 array the maximum size of this AMC surface.

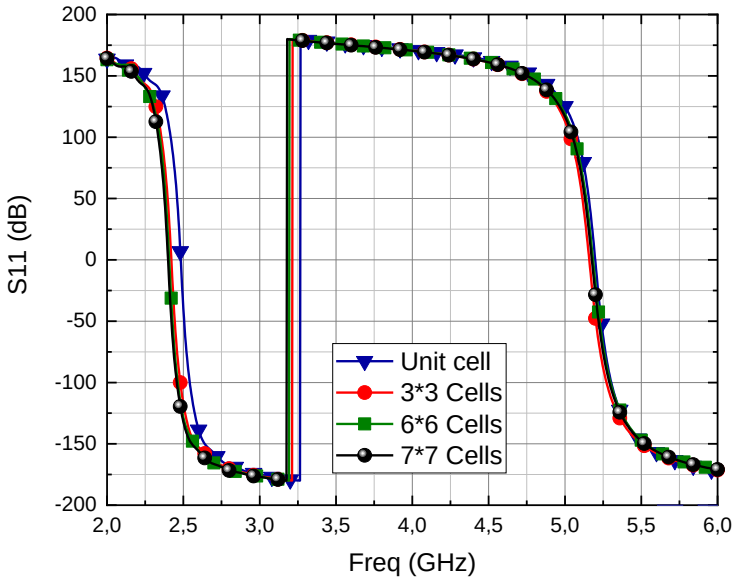

Figure 3.13 Reflection phase of different AMC surface size.

The simulated surface impedance of 6 by 6 AMC structure is represented in Figure 3.14. It can be seen that the AMC structure acts as a high impedance surface at the desired resonant reflective bands, such that it achieves 988 Ω and 1028 Ω respectively, which is higher than the surface impedance of the unit cell.

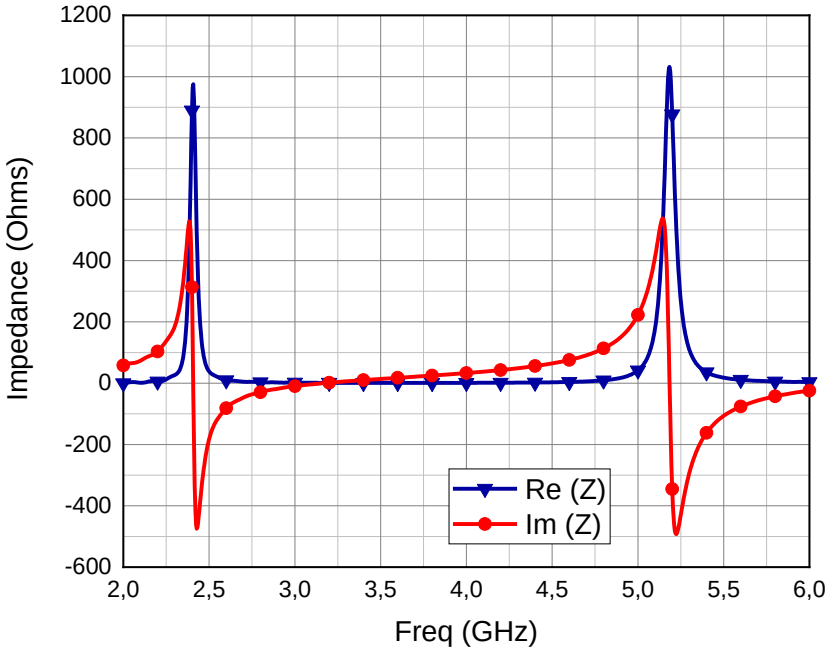

Figure 3.14 Surface impedance of the 6 by 6 AMC structure.

Figure 3.15 shows the simulated current distribution of the 6 by 6 AMC surface at the frequencies 2.45 GHz and 5.20 GHz .The current is seen to be distributed in the entire AMC surface at the first frequency, whereas at second frequency the current is concentrated at the inner circular patch as it has been seen in the unit cell.

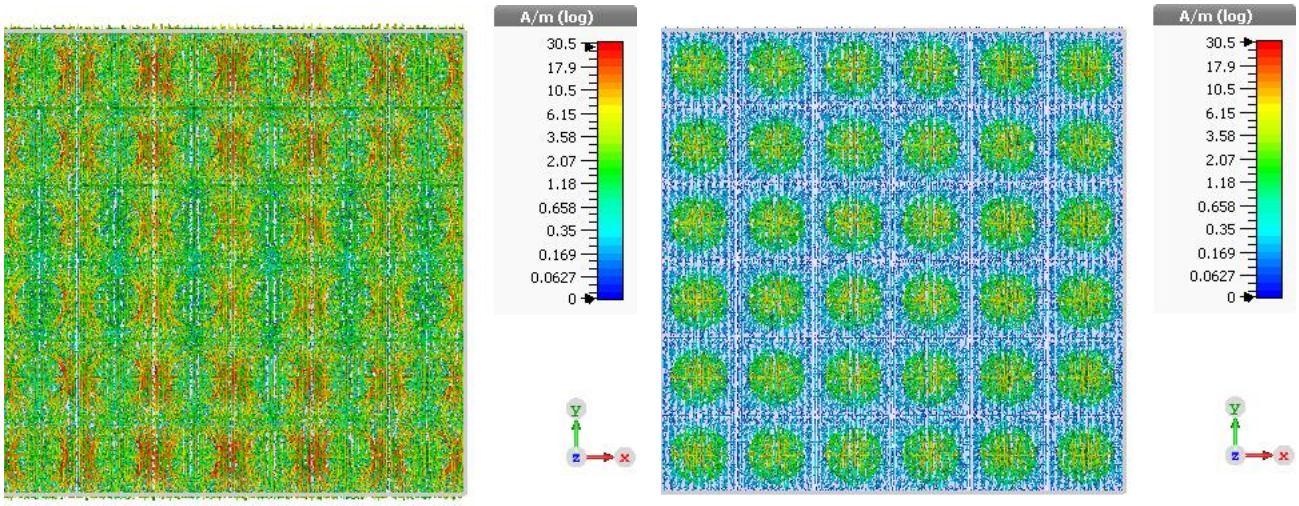

(a) **(b)**

Figure 3.15 Current distribution of the 6 by 6 AMC structure at,

(**a)** 2.45 GHz (**b)** 5.20 GHz.

3.4 Conclusion

In this chapter, a novel Dual band AMC unit cell has been designed and analyzed to have an in-phase reflection property for a plane wave of normal incidence at 2.45 GHz and 5.20 GHz. Several parametric studies have been conducted in order to achieve the optimum design. In addition, it has been found that the AMC structure at both higher and lower resonant frequencies behaves as a high impedance surface. These results will be exploited to improve the performance of the dual band antenna in the next chapter.

CHAPTER 04

Gain Enhancement Using High Impedance Surface

CHAPTER 04: Gain Enhancement Using High Impedance Surface

4.1 Introduction

Microstrip antenna is characterized by light weight, thin profile and low fabrication cost, but offers low gain. In this chapter, the proposed AMC surface is used as a ground plane reflector in order to enhance the gain of the CPW antenna without affecting the other parameters such as impedance bandwidth and return loss. In contrast to many researches on single-band low profile antenna design, the work focuses on improving the CPW antenna's radiation performance within two operating bands simultaneously by using a dual in-phase reflection band AMC for two practical frequency bands centered at 2.45 GHz and 5.20 GHz.

4.2 Monopole antenna loaded with AMC surface

In order to improve the gain, an AMC reflector is added under the CPW antenna. This reflector is an array of AMC unit cells that is described in chapter 3 and its overall size is 11.4×11.4 cm^2. The antenna is placed above the reflector in the middle at a distance of d. A thin foam layer with thickness d, relative permittivity of 1.01 and loss tangent of 1.1×10^{-4} is put between the AMC reflector and the CPW antenna as illustrated in Figure 4.1.

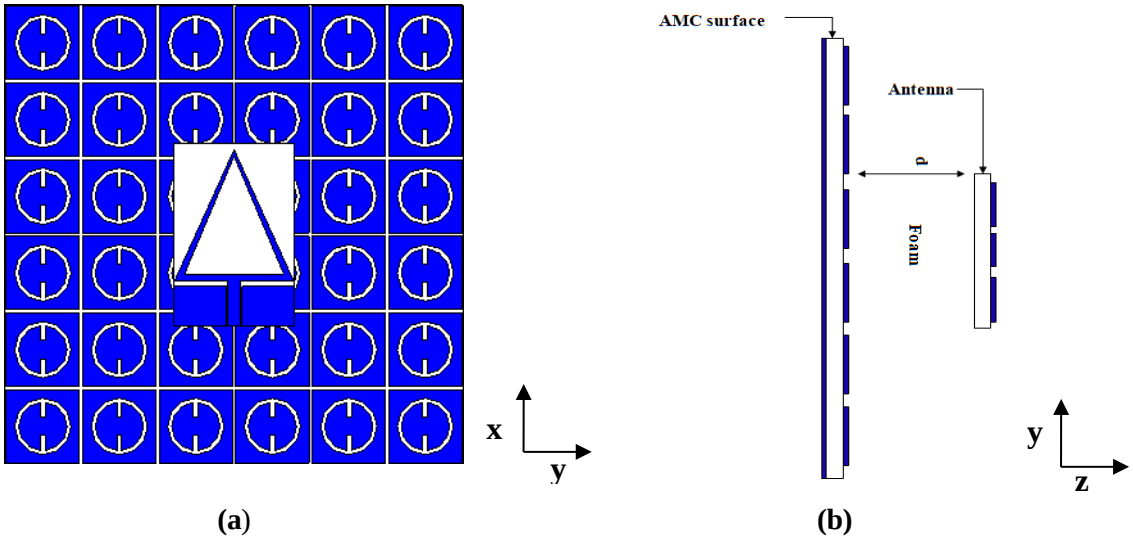

Figure 4.1 Configuration of CPW antenna with an AMC reflector**,**
(a) top view **(b)** Side view.

4.3 Simulation and Results

The performance of the antenna over the AMC surface was studied by carrying out the detailed parametric analysis to visualize the behavior of the input reflection coefficient, the efficiency, the radiation pattern and the current distribution.

4.3.1 Distance impact on The Antenna Performance

In this section, the impact of the distance between the antenna and AMC reflector on the antenna performance is studied by varying the distance from 5 to 50 mm. Figure 4.2 shows the simulated realized gain and directivity versus the distance between the antenna and the AMC surface at 2.45 GHz and 5.2 GHz. The realized gain and directivity are clearly related to the distance between the antenna and the reflector. At the lower resonant frequency, the realized gain is maximum about 7.29 dBi at a distance of 14 mm then decreases until 36 mm then it increases again; whereas at the higher resonant frequency, the realized gain has two maxima about

7.89 dBi and 7.78 dBi at 14 mm and 43 mm respectively because its wavelength is very small compared with the first resonant frequency, therefore the second maxima is rapidly achieved. The directivity is extremely high and very far from the realized gain when the antenna is more closed to the AMC surface, as the distance increases the directivity becomes closer to the realized gain at both resonant frequencies. As a result, the losses and mismatch occur as the antenna becomes closer to the AMC sheet.

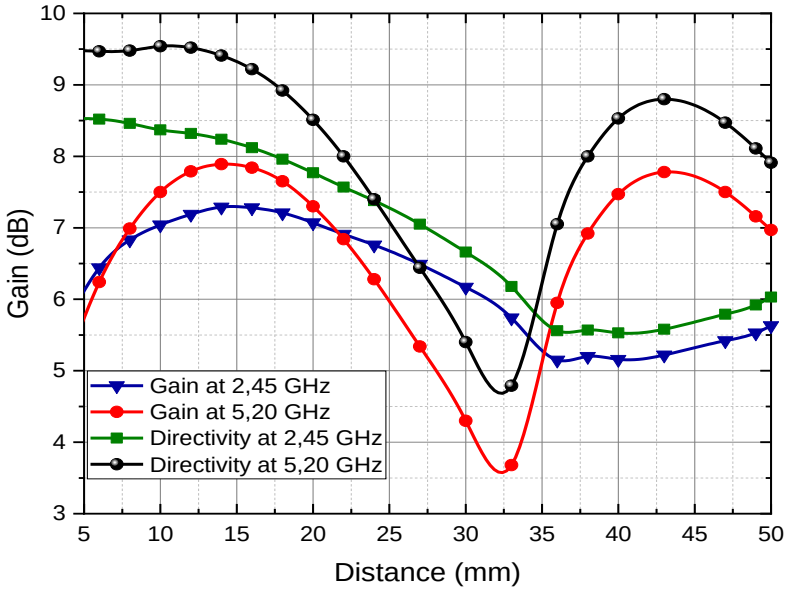

Figure 4.2 Simulated realized gain and directivity versus distance.

Figure 4.3 shows the efficiency versus the distance between the antenna and the AMC surface at 2.45 GHz and 5.20 GHz. At the lower resonant frequency, the reflection efficiency is low as the antenna is much closer to the AMC surface, due to the high electromagnetic interference among the antenna and the AMC surface that causes the mismatch loss. While at the higher resonant frequency, the reflection efficiency is very high for all the distances from 5 mm to 50 mm which makes the matching achieved. Whereas the radiation efficiency increases at both resonant frequencies as the distance increases, therefore the antenna efficiently radiates the input power in the higher distances and the power is mostly dissipated in the lower distances. As a result, the total efficiency increases with an increase in distance; Notice that the total efficiency at the first resonant frequency is higher than the second one.

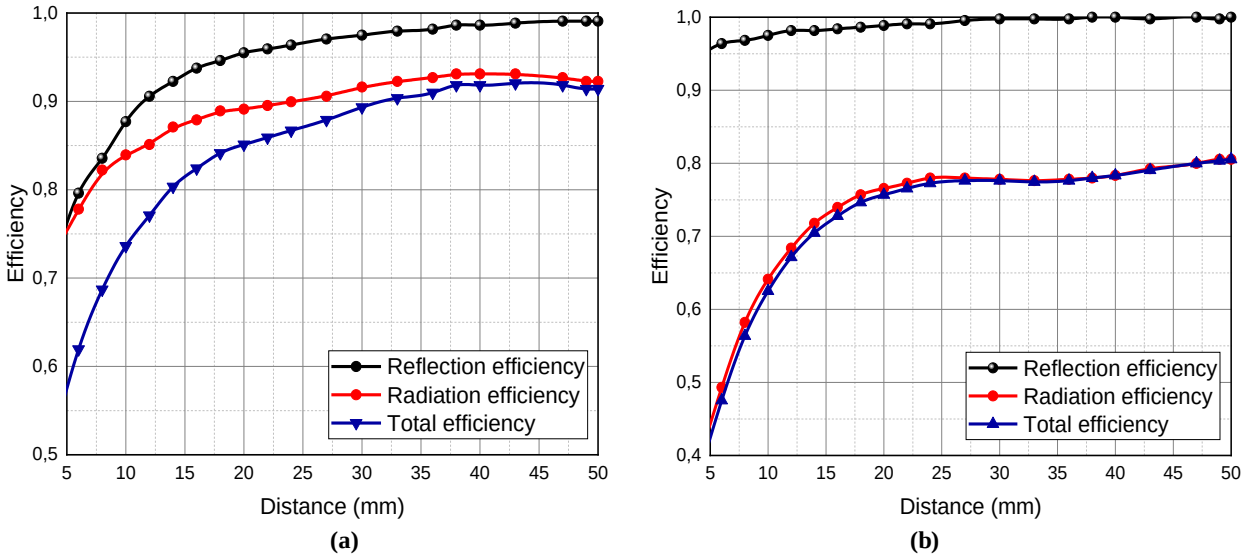

Figure 4.3 Simulated efficiency versus distance at **(a)** 2.45 GHz (**b)** 5.2 GHz.

The E plane and H plane radiation patterns at 2.45 GHz and 5.2 GHz for different distances are shown in Figure 4.4 and Figure 4.5, respectively. It can be seen that increasing and decreasing the distance between the antenna and the AMC reflector gives a distinct radiation patterns that differ in the peak gain and directivity.

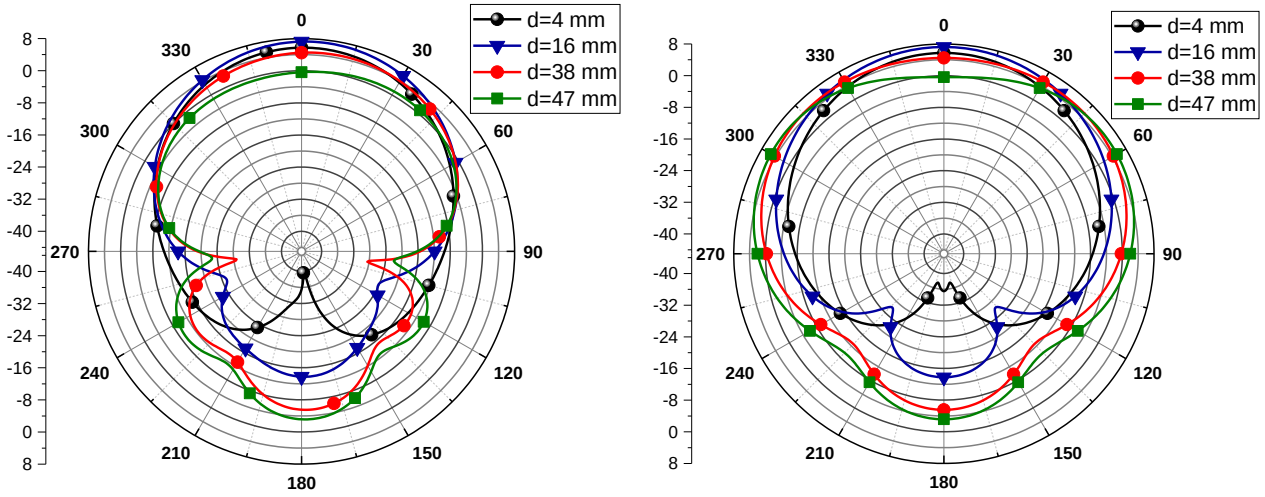

Figure 4.4 Simulated radiation patterns at 2.45 GHz, **(a)** E plane **(b)** H plane.

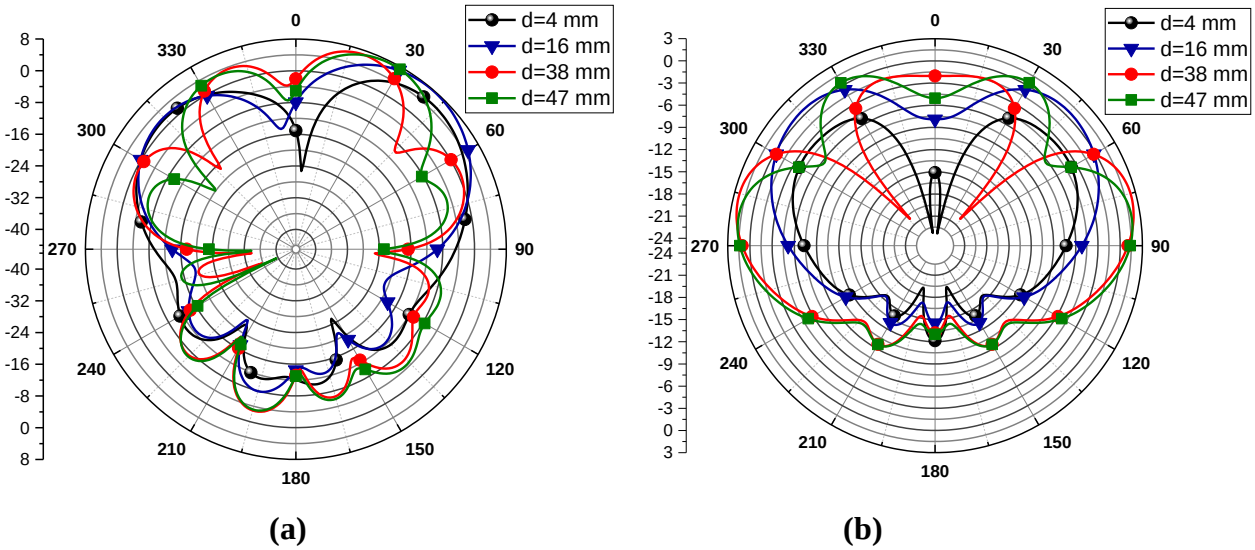

Figure 4.5 Simulated radiation patterns at 5.2 GHz, **(a)** E plane **(b)** H plane.

The input reflection coefficient of the monopole antenna at different distances from the AMC surface is shown in Figure 4.6; noting that the chosen distances ensure a high gain as it has seen in Figure 4.2. It can be observed that the bandwidth and the impedance matching are affected by the parameter d. As the distance d increases the bandwidth of the lower resonant frequency increases and the coupling between the antenna and the AMC surface decreases which leads to a good impedance matching [27]. While at the higher resonant frequency, the bandwidth remains unchanged and the matching is good at all the selected distances since the input reflection coefficient is less than $-10\ dB$.

Remark: The distance $16\ mm$ (about $0.13\ \lambda$) has been selected to continue the analysis of the monopole antenna over the AMC surface, taking into consideration the high gain with better bandwidth and impedance matching without getting out from the low profile design.

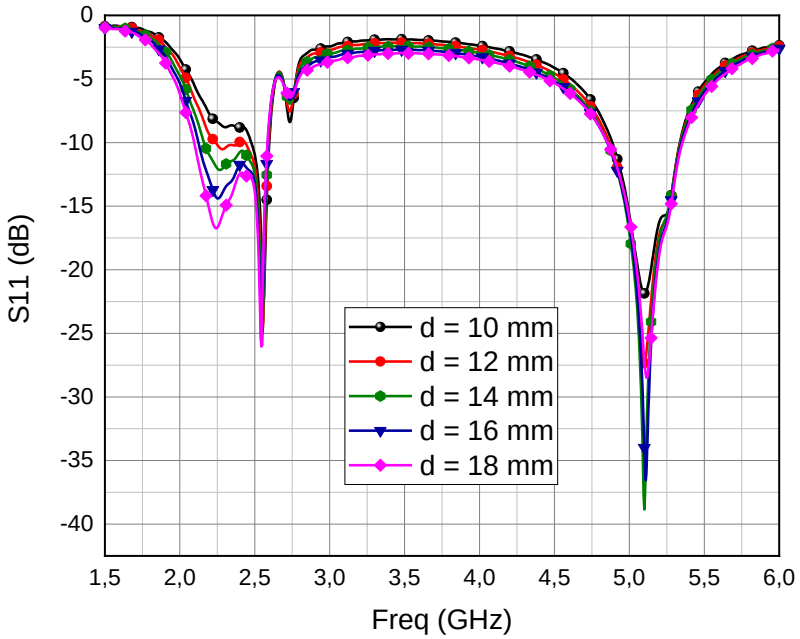

Figure 4.6 Simulated input reflection coefficient of the CPW antenna at different distances from the AMC surface.

4.3.2 AMC Size Impact on the Antenna Performance

In this section, the effect of the AMC surface size is discussed. The analysis is made for a fixed distance $d = 16\ mm$.

Figure 4.7 represents the simulated input reflection coefficient of different sizes of the AMC surface. It appears that the number of AMC unit cells mainly affects the lower resonant frequency band, so that as the number of unit cells increases the lower resonant frequency is shifted to the left towards the desired operating frequency with better impedance matching and bandwidth .

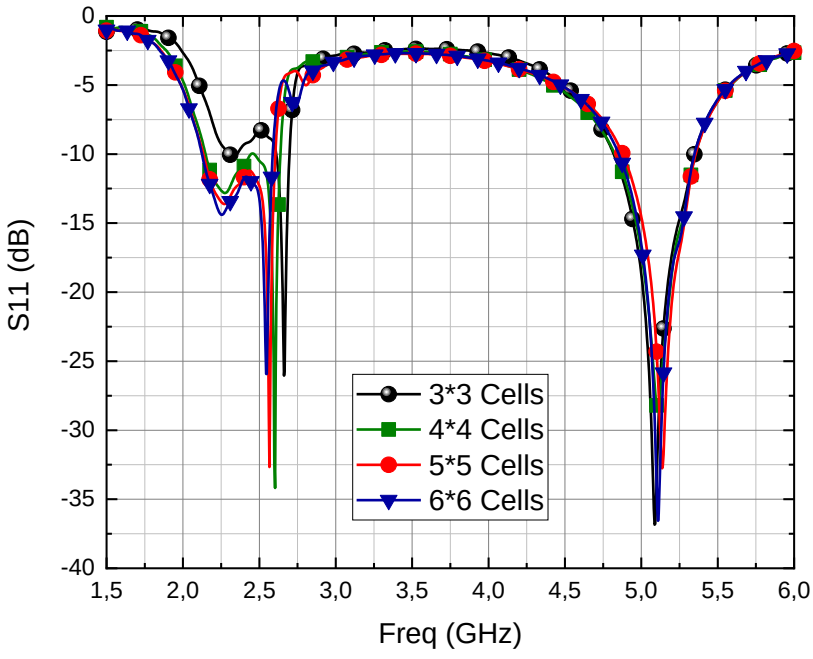

Figure 4.7 Simulated input reflection coefficient for the monopole antenna for different sizes of AMC surface.

The E plane and H plane radiation patterns at 2.45 GHz and 5.20 GHz of different AMC surface sizes are depicted in Figure 4.8 and Figure 4.9, respectively. The results are summarized in table 4.1 and table 4.2.

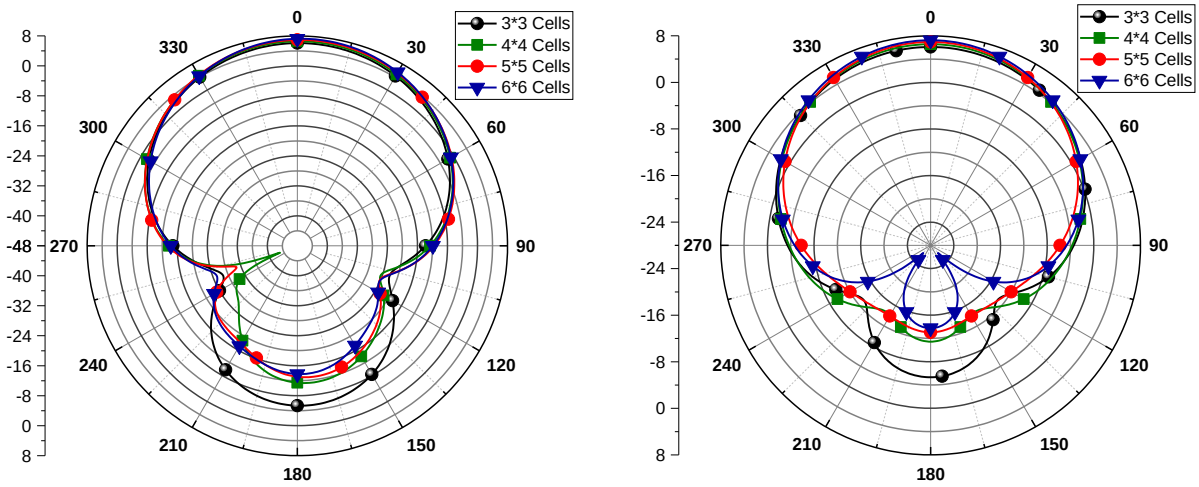

Figure 4.8 Simulated radiation patterns for different sizes of AMC surface at 2.45 GHz, **(a)** E plane **(b)** H plane.

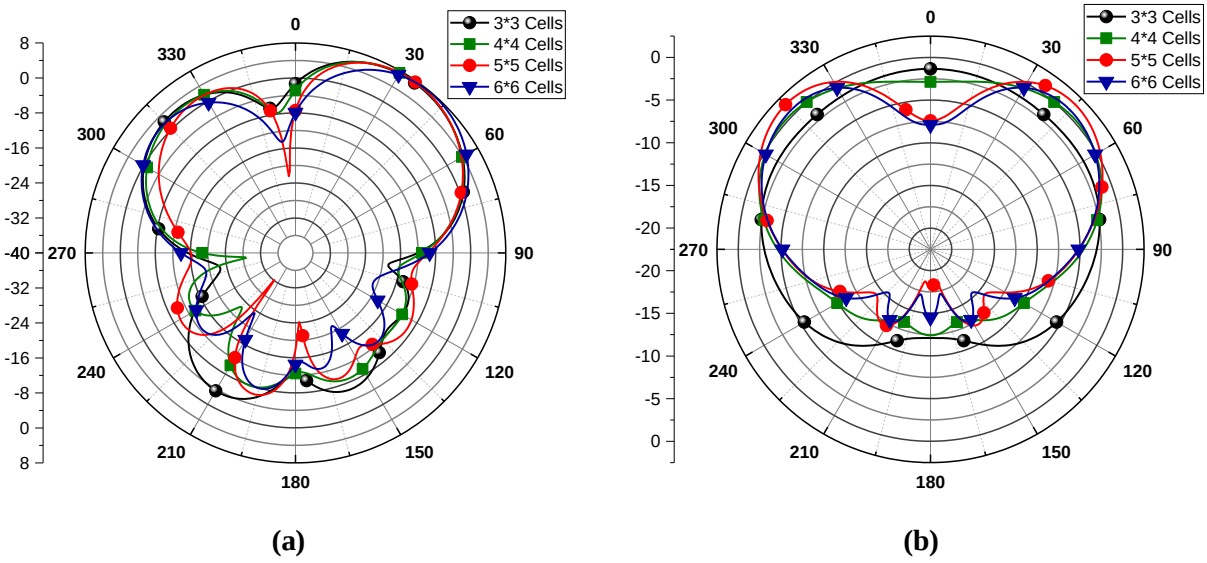

Figure 4.9 Simulated radiation patterns for different sizes of AMC surface at 5.2 GHz, (a) E plane **(b)** H plane.

Table 4.1Simulated results of the antenna over different sizes of AMC surface at 2.45 GHz.

	Realized Gain (*dBi*)	**Directivity (*dBi*)**	**Beamwidth (*degree*)**	**Back lobe level (*dBi*)**
3×3 ***cells***	6.08	7.24	74.2	-11.4
4×4 ***cells***	6.56	7.47	74.2	-17.9
5×5 ***cells***	6.96	7.75	72.4	-19.8
6×6 ***cells***	7.28	8.12	67.7	-21

Table 4.2 Simulated results of the antenna over different sizes of AMC surface at 5.2 GHz.

	Realized Gain (*dBi*)	Directivity (*dBi*)	Beamwidth (*degree*)	Side lobe level (*dBi*)
$3 \times 3 cells$	7.41	8.47	46.3	-4.9
$4 \times 4 cells$	7.61	8.82	43.6	-5.4
5×5 *cells*	7.66	8.88	42.0	-6.0
6×6 *cells*	7.84	9.22	39.7	-5.8

According to the tables 4.1 and 4.2, it can be seen that the realized gain at both resonant frequencies is improved as the number of unit cells increases, while the secondary lobe level is minimized and the beamwidth is reduced resulting in an increase in the directivity.

Remark: Based on the above analysis of the effect of the AMC surface size on the antenna performance and according to the obtained results, a 6×6 AMC array has been selected since it offers higher gain and better impedance matching at the desired resonant frequencies.

4.2.3 The Optimum Design for Monopole Antenna Loaded With AMC Surface

The CPW monopole antenna is employed on an AMC surface consisting of 6×6 unit cells.The separation distance between the antenna and the artificial magnetic conductor is maintained to be $16\,mm$ for a proper impedance matching and a suitable gain pattern. The simulated input reflection coefficient of the antenna with and without AMC plane in free space is illustrated in Figure 4.10.

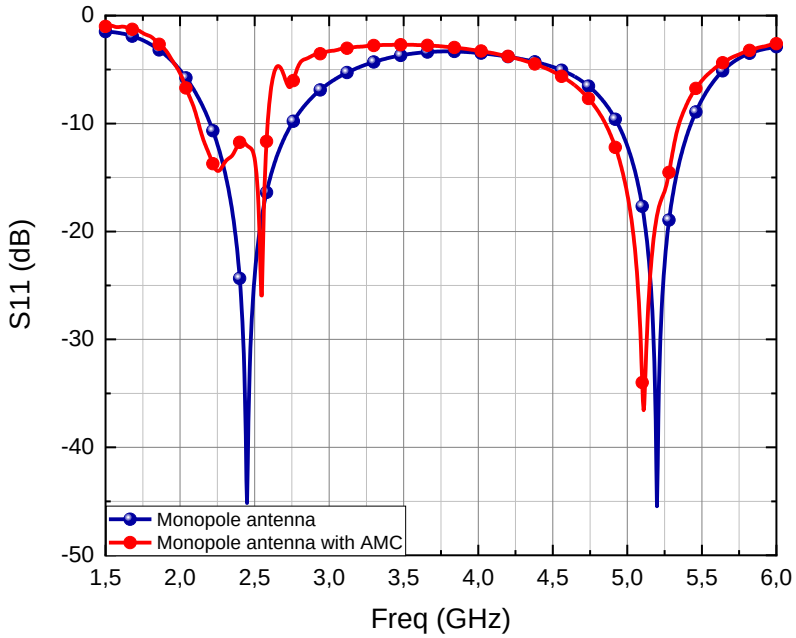

Figure 4.10 Simulated input reflection coefficient for the monopole antenna with and without AMC surface.

From the above figure, it can be seen that the input reflection coefficient of the CPW antenna with AMC structure provides a good matching at the desired operating frequencies about $-12.05\,dB$ and $-18.46\,dB$ which are less than $-10\,dB$ with high bandwidth of 463.38 MHz and 495.79 MHz at 2.45 GHz and 5.2 GHz, respectively. Compared with the input reflection coefficient of the monopole antenna without AMC sheet, there is a slightly change in the higher resonant frequency that is moved to the left. However, at the lower frequency band a new resonant frequency is generated after introducing the AMC surface, this change is due the mutual coupling effect between the antenna and the AMC surface as it has mentioned before.

The simulated E plane and H plane radiation patterns of the CPW antenna over AMC surface at 2.45 GHz and 5.2 GHz are displayed in Figure 4.11 and Figure 4.12, respectively. It is clearly seen that after placing the AMC surface under the antenna by a distance of $16\ mm$ the realized gain is well enhanced ,the directivity is increased and the radiation patterns become unidirectional ;so that at the lower frequency ,the realized gain is increased by $5.01\ dBi$ in the E plane with a beamwidth of $67.7°$ and by $4.99\ dBi$ in the H plane with a beamwidth of $85.5°$. Whereas at the higher frequency, the realized gain is raised by $5.62\ dBi$ in the E plane with beamwidth of $39.7°$ and by $0.36\ dBi$in the H plane with beamwidth of $54.1°$.

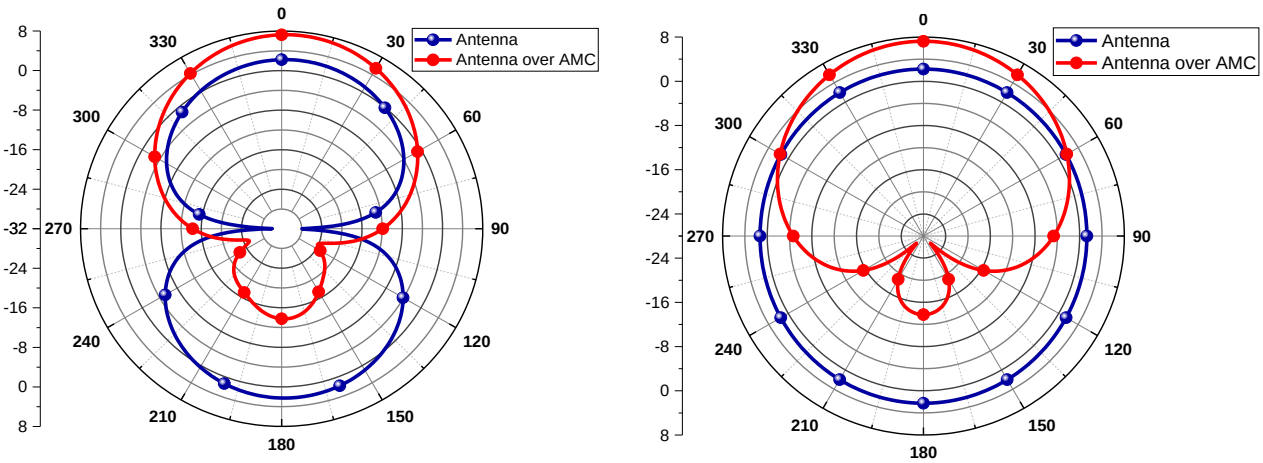

(a) **(b)**

Figure 4.11 Simulated radiation patterns of the CPW antenna with and without AMC surface at 2.45 GHz, **(a)** E plane **(b)** H plane.

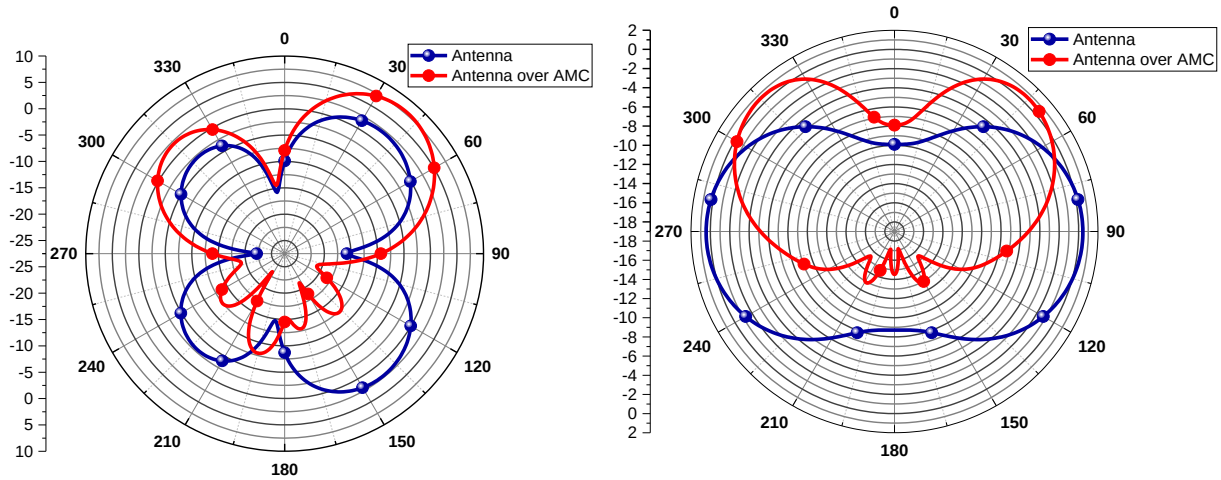

(a) **(b)**

Figure 4.12 Simulated radiation patterns of the CPW antenna with and without AMC surface at 5.2 GHz, **(a)** E plane (**b)** H plane.

Figure 4.13 shows the simulated 3D radiation patterns of the CPW antenna over AMC surface at 2.45 GHz and 5.20 GHz. Compared to the radiation patterns of the reference antenna that has been shown in Figure 2.12 ,it is clearly observed that the final design is unidirectional and the gain is well enhanced as indicated before.

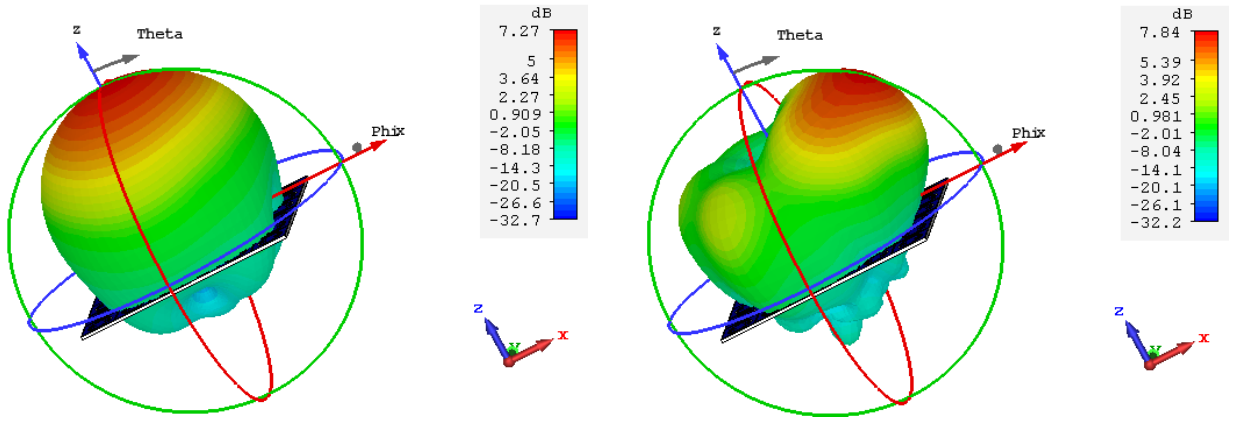

(a) **(b)**

Figure 4.13 Simulated 3D radiation patterns of the CPW antenna over AMC surface at **(a)** 2.45GHz (**b)** 5.20 GHz.

Figure 4.14 shows the current distribution of the antenna over the AMC surface at 2.45 GHz and 5.20 GHz. Compared to the current distribution of the original antenna, the flow of current rotating around the radiating patch is improved and the current intensity is increased due to the interaction and excitation of the AMC cells on the antenna contributing to the radiated field.

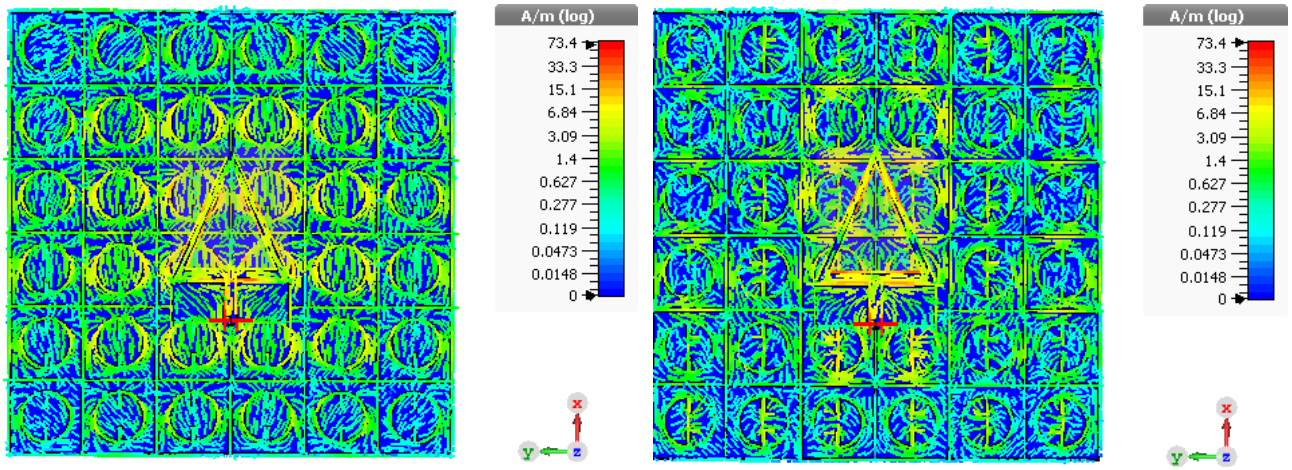

(a) **(b)**

Figure 4.14 The current distribution of the CPW antenna over AMC surface at **(a)** 2.45 GHz **(b)** 5.20 GHz.

The plots of different types of efficiency versus frequency of the CPW antenna over AMC surface are represented in Figure 4.15. It can be seen that the efficiency is high at both operating frequency bands. The reflection efficiency reaches 0.937 at 2.45 GHz and 0.985 at 5.2 GHz, while the radiation efficiency achieves 0.878 at the lower frequency and 0.739 at the higher frequency, which results in a high total efficiency of 0.824 and 0.728 at the first and second frequencies, respectively.

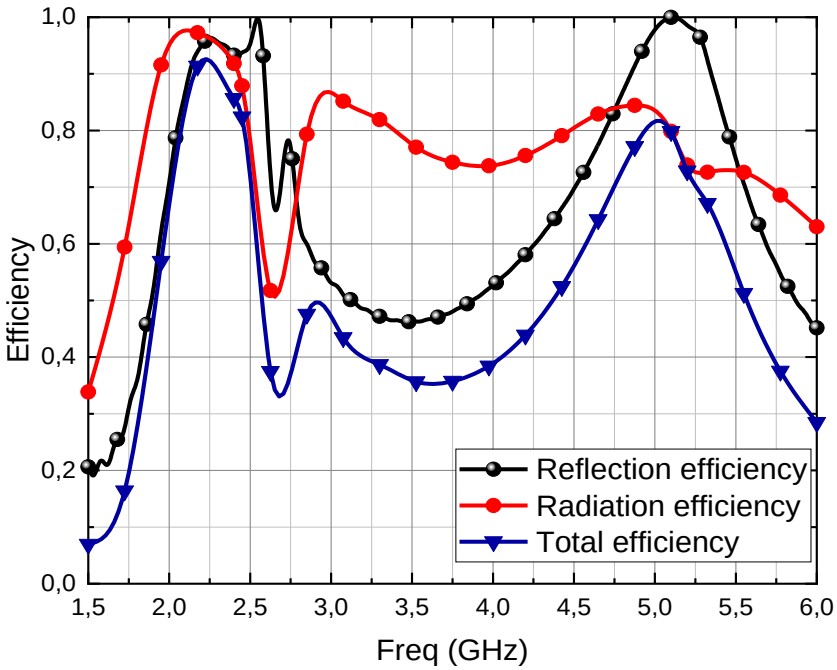

Figure 4.15 Antenna efficiency versus frequency of the CPW antenna over AMC surface.

For comparison, the input reflection coefficient of the CPW antenna over AMC surface, AMC antenna over large metal (300mm×300mm) and antenna over PEC are simulated and depicted in Figure 4.16. It can be observed that a mismatch occurs at the lower frequency band where the input reflection coefficient is greater than -10 dB after changing the AMC surface by a PEC sheet .However, adding the large metal to the AMC antenna does not affect the resonant frequencies, the bandwidth remains the same and the design still have a good matching at the desired frequencies. Furthermore, the gain is almost preserved as it is shown in table 4.3.Consequently, it can be concluded that the AMC surface electromagnetically insulates the antenna from the metallic plate without disturbing the antenna performance.

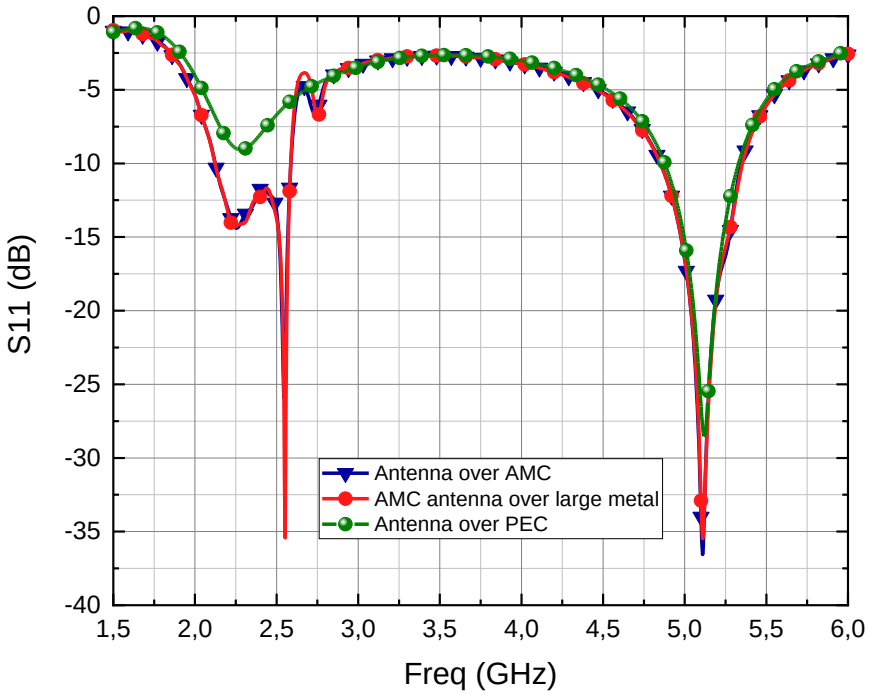

Figure 4.16 Simulated input reflection coefficient for various cases.

Table 4.3 Simulated antenna performances at 2.45 GHz and 5.20 GHz .

.

	f = 2.45 GHz			f = 5.20 GHz		
	Realized Gain (*dBi*)	Directivity (*dBi*)	Total Efficiency (%)	Realized Gain (*dBi*)	Directivity (*dBi*)	Total Efficiency (%)
Antenna alone	2.27	2.48	95	2.22	3.13	81
Antenna with AMC	7.28	8.12	82	7.84	9.22	73
Antenna with AMC over large metallic plate	7.64	8.44	83	7.4	8.66	75

4.4 Conclusion

In this chapter, a dual band CPW monopole antenna is integrated with a dual band AMC reflector. It has been shown that the distance between the antenna and the AMC surface and also the AMC size have a big impact on the antenna performances. The radiation performances including antenna gain, directivity and radiation pattern are significantly improved as a contrast to the reference CPW antenna. The gain enhancement can be up to more than $5\ dBi$. The final design is a dual band CPW antenna over a 6×6 AMC surface by a distance of 16 mm which shows a unidirectional radiation at the two operating frequencies simultaneously, the gain reaches $7.28\ dB$ and $7.84\ dB$ at 2.45 GHz and 5.2 GHz, respectively and the input reflection coefficient attains $-12.05\ dB$ with bandwidth of 463.38 MHz and $-18.46\ dB$ with bandwidth of 495.79 MHz at the lower and higher operating frequencies, respectively. The investigations show that placing the AMC antenna over a large metallic plate does not change the performances of the antenna. Overall the results are acceptable and the goal is achieved.

Conclusion and Suggestions For Further Work

Conclusions and Suggestions for Further Work

In this project, an efficient solution to enhance the gain of dual band microstrip antenna is proposed. In the first part, the design of novel dual band CPW monopole antenna has been designed to cover the WLAN bands (2.4 GHz, 5.20 GHz). The second part deals with the design of dual band AMC unit cell operating at 2.45 GHz and 5.20 GHz reflection bands. In the last part, loaded CPW monopole antenna with AMC surface is studied for gain enhancement.

Conclusions

The theory behind microstrip antenna and its parameters have been initially introduced beside to the topic of metamaterials that has been discussed briefly. Then a triangular ring patch antenna has been designed with a coplanar feed line and the verification of the parameters of the proposed patch antenna has been performed. The aim was to study a novel structure to achieve a dual band antenna that resonates at 2.45 GHz and 5.20 GHz covering WLAN applications with large bandwidth and high impedance matching.

The obtained results showed a good agreement in the operating bands which meet the requirements of WLAN applications. In addition, the proposed antenna had an omnidirectional radiation pattern at the lower resonant frequency with realized gain of $2.27\ dBi$ and directivity about $2.48\ dBi$ and bidirectional radiation pattern at the higher resonant frequency with gain of $2.22\ dBi$ and directivity about $3.11\ dBi$.

The work followed by designing the AMC unit cell that reflects the two resonant frequencies simultaneously without phase shift. To achieve the optimum design, a comparative study was carried out on the effect of various parameters on the unit cell performances. The investigations indicated that the in phase reflection band was about 104 MHz and 183 MHz at the lower and higher frequency bands, respectively.

After making an array of the proposed unit cell, it has been positioned beneath the proposed microstrip antenna. Then, an analysis on the AMC size and antenna-AMC distance impact has been done. The final structure was a dual band antenna separated from a 6×6 AMC surface by a distance of 16 mm. This design, as expected increased the gain significantly as a contrast to the reference coplanar antenna, the enhancement might exceed $5\ dB$. Moreover, it also improved the radiation pattern by increasing the directivity.

Suggestions for further work

Throughout the development of this project, many possible issues have been opened to extend the study of microstrip antenna as well as the metamaterial structures according to the desired applications. Some possible future research directions for the work reported on this project are discussed here:

- Experimental investigation for the proposed antenna loaded with AMC surface.
- New size reduction methods need to be investigated to satisfy the size and band specifications of the communications systems nowadays.
- As final suggestion, extend the use of high impedance surface to the biomedical domain, by study it with antennas integrated on cloths to reduce the radiation back face, thus reducing the value of the specific absorption rate in the presence of the human body.

References

References

[1] A. Kumar, and D. Kumar V, " High-performance Metamaterial Patch Antenna," *Microwave and Optical Technology Letters* , vol. 55 ,pp.409–413, February 2013.
[2] P. Prakash, M. P. Abegaonkar, A. Basu, and S. K. Koul, "Gain enhancement of a CPW-fed monopole antenna using polarization-insensitive AMC structure," *IEEE Antennas and Wireless Propagation Letters*, vol. 12, pp. 1315-1318, 2013.
[3] R. C. Hadarig, de Cos, M.E, and Las-Heras, F, "Novel Miniaturized Artificial Magnetic Conductor," *IEEE Antennas and Wireless Propagation Letters*, vol. 12, pp.174-177, January 2013.
[4] Anuj Mehta,"Microstrip antenna," *International Journal Of Scientific & Technology Research*, Vol.4, Issue 03, March 2015.
[5] B. Gireesha, Layak Ali,"MATLAB/Simulink and CST Software based Efficiency Improved Square Patch Microstrip Antenna with PSO Algorithm," *Jour of Adv Research in Dynamical & Control Systems*, Vol. 11, 06-Special Issue, 2019.
[6] Vivek Hanumante, Sahadev Roy,"Comparative Study of Microstrip Patch Antenna Using Different Dielectric Materials,"*9th International Conference on Microwaves, Antenna, Propagation and Remote Sensing ICMARS-2013*, Jodhpur, INDIA, 11th – 14th December, 2013.
[7] K.DJAFRI," Contribution to the Study and Design of Miniaturized Microstrip Antennas",PhD Thesis ,IEEE/ University M'Hamed BOUGARA, Boumerdes, 2018/2019.
[8] Narinder Sharma, Navpreet Kaur, Navdeep Singh," A Study Of Different Feeding Mechanisms In Microstrip Patch Antenna," *International Journal of Microwaves Applications*, vol.6, No.1, January – February 2017.
[9] F.GUICHI,"Study and Design of Planar Antennas for UWB Application",PhD Thesis ,IEEE/ University M'Hamed BOUGARA, Boumerdes, 2018.
[10] Ali Elrashidi, Khaled Elleithy, Hassan Bajwa," Input Impedance, VSWR and Return Loss of a Conformal Microstrip Printed Antenna for TM01 Mode Using Two Different Substrates," *International Journal of Networks and Communications*, vol. 2,no.2,pp. 13-19 ,2012.
[11] C. A. Balanis, "Antenna theory: analysis and design", 4th edition, John wiley & sons, Hoboken, New Jersey, 2016.
[12] P. A. Azrar, "Antennas "Fundamental Parameters Of Antennas"," Igee/Umbb ,Boumerdes, Algeria.
[13] R.Marques ,F.Martin, M.Sorolla, Metamaterials with Negative Parameters :Theory, Design, and Microwave Applications, John Wiley & Sons New York, 2008.
[14] Josep, Canet-Ferrer, Metamaterials and metasurfaces, IntechOpen, London, United Kingdom, 2019.
[15] Sangeeta Chakrabarti,"Controlling Metamaterials with Radiation and Controlling Radiation with Metamaterials,"PhD Thesis,Departement Physics/Indian Institute Of Technology Kanpur,INDIA,2010.
[16] Xingcun Colin,Tong,Functional metamaterials and metadevices, Springer International Publishing,2018.
[17] Ben A. Munk, Frequency Selective Surface: Theory and Design, John Wiley &Sons,New York, 2000.
[18] Jay Houston Barton, "Frequency Selective Surfaces For Extreme Applications," PhD thesis,Texas at El PasoUniversity, El Paso, May 2014.

[19] https://www.tutorialspoint.com/antenna_theory/antenna_theory_slot.htm.

[20] F.Mouhouche, “Study and Analysis of Metameterials Antenna structures,”PhD thesis,Igee/umbbUniversity, Boumerdes,Algeria, 2019.

[21]http://www.mweda.com/cst/cst2013/mergedProjects/CST_PARTICLE_STUDIO/special_overview/special_overview_waveguideover.htm.

[22] F. Mouhouche, A. Azrar, M. Dehmas, and a. K.Djafri, "Gain Improvement of CPW-Fed Monopole Antenna over Dual-Band AMC Structure," *2017 5th International Conference on Electrical Engineering - Boumerdes (ICEE-B)*, 2017.

[23] http://www.edatop.com/cst/CST2013/30592.html.

[24] H. T. Qun Luo, Zhitong Huang, Xudong Wang, Zheng Guo, andYuefeng Ji, "Unidirectional Dual-Band CPW-Fed Antenna Loaded withan AMC Reflector,"*International Journal of Antennas and Propagation*,2013.

[25] Yu Zhu, “Modeling of High Impedance Surface Structures,” PhD thesis ,Paris –Sud XI University ,2011.

[26] D. Sievenpiper, L. Zhang, R. F. J. Broas, N. G. Alexopolous, and E. Yablonovitch, “High-impedance electromagnetic surfaces with a forbidden frequency band,” *IEEE Trans. Microwave Theory & Tech.*, vol. 47,no. 11, pp. 2059–2074, Nov. 1999.

[27] Xue-Yan Song, Chuang Yang, Tian-Ling Zhang, Ze-Hong Yan, and Rui-Na Lian “ Broadband and Gain Enhanced Bowtie Antenna with AMC Ground,” *Progress In Electromagnetics Research Letters, Vol. 61, pp.25–30, 2016.*

[28] Frank Gustrau, RF and Microwave Engineering: Fundamentals of Wireless Communications, John Wiley & Sons Ltd, Chichester, UK, 2012.

Appendix A

APPENDIX A: Coplanar Line

A.1 Definition

In a coplanar line, the metallic strip (width w) runs between infinite ground planes separated by slots (slot width s) on the upper surface of a substrate. In real circuits the ground planes have finite width $w_g > w$. Strip and ground are located in the same plane, hence, the name coplanar. Figure A.1 shows the geometry. The trace represents the signal conductor and the ground planes represent the return conductors [28]. The distance d between the ground planes is:

$$d = w + 2s \tag{A-1}$$

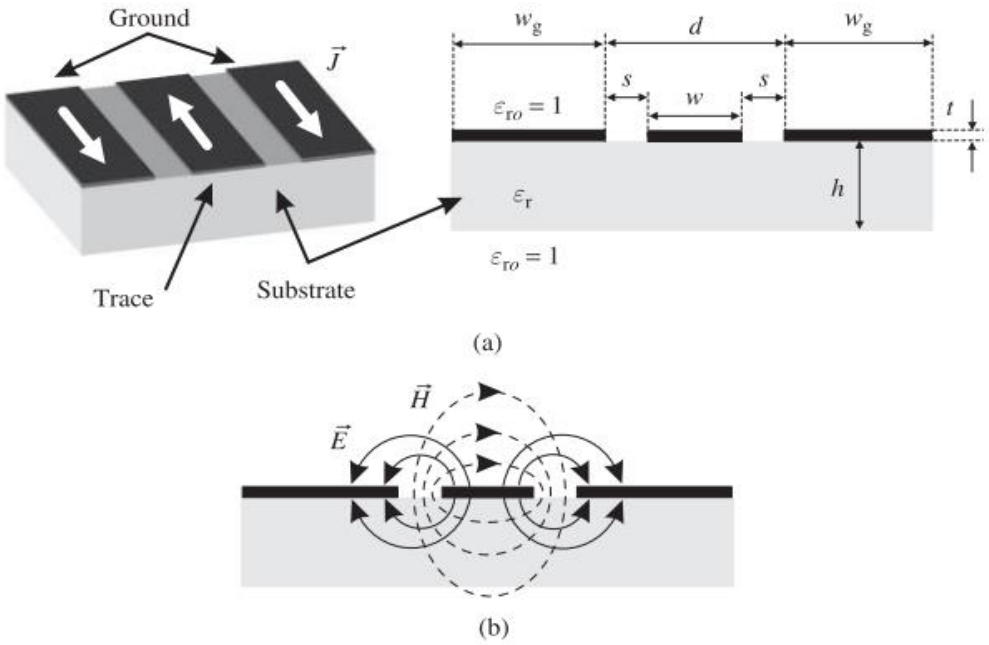

Figure A.1 (a) Geometry of a coplanar transmission line **(b)** electric and magnetic field distribution of a quasi-TEM wave.

An electromagnetic wave is present in air and substrate (height h, relative permittivity ε_r, so the fundamental wave type is quasi-TEM (see figure A.1), where the magnetic fields runs in closed loops around the center conductor and the electric fields point from center conductor to the ground planes [28].

A.2 Characteristic Impedance and Effective Permittivity

First, let us assume that we have low frequencies defined by a distance d between the ground planes. This distance shall be small compared to a quarter wavelength of an electromagnetic wave inside the substrate

$$d \ll \frac{\lambda_0}{4\sqrt{\varepsilon_r}} \tag{A-2}$$

Where $\lambda_0$is the free space wavelength.

For thick substrates (substrate height h much greater than total line width d).the electromagnetic wave is distributed over air and substrate in equal shares. Hence, the effective relative permittivity is

$$\varepsilon_{r,eff,thick} = \frac{\varepsilon_r + 1}{2} \tag{A-3}$$

If the substrate becomes thinner, a greater part of the wave is in air; hence the effective relative permittivity gets smaller [28].

Approximate expressions for the characteristic impedance Z_0 are given as:

$$Z_0 = \begin{cases} \frac{120\Omega}{\sqrt{\varepsilon_{r,eff,thick}}} ln\left(2\sqrt{\frac{d}{w}}\right) & \text{for } \frac{w}{d} \leq 0.17 \\ \frac{30\pi^2\Omega}{\sqrt{\varepsilon_{r,eff,thick}}}\left[ln\left(2\frac{1+\sqrt{w/d}}{1-\sqrt{w/d}}\right)\right]^{-1} & \text{for } \frac{w}{d} \geq 0.17 \end{cases} \quad \text{(A-4)}$$

A.3 Designing Coplanar Line

One of the key building blocks in constructing a MATLAB simulation is the ability to write custom user functions. To demonstrate this, a function that plots the characteristic impedance of coplanar line versus $\frac{w}{d}$ for given value of relative permittivity ε_r is created. The purpose is to find the optimum ratio to get $Z_0 = 50\ \Omega$. Then this ratio is used to plot width of coplanar strip line w versus slot width s.
The following MATLAB program gives a the complete process:

MATLAB Code A.1

```
function[Z0,ratio] = Z0_characteristic(epsi_r,S)
%====================================================================
%epsi_r= relative permitivity
%w=width of strip line
%s=slot width
%S=the range of slot width
% Z0 = characterstic impedance
%epsi_reff=  =  Effective relative permitivity
%Ratio=w/d where d=w+2s
%====================================================================
%plotting the characterstic impedance versus the ratio w/d
ratio=0.001:0.0001:1;
    epsi_reff=(epsi_r+1)/2
if(ratio)<=0.17
    Z0=(120/sqrt(epsi_reff)).*log(2*sqrt(1./ratio));
else
    Z0=(30*pi^2./sqrt(epsi_reff))./log(2*((1+sqrt(ratio))./(1-
sqrt(ratio))));
end
 plot(ratio,Z0,'b','linewidth',2)
 grid
 title(' Characteristic impedance versus the ratio w/d')
 xlabel('ratio w/d')
 ylabel('Z0(ohms)')
 figure
 %====================================================================
 %plotting width w versus slot width s for Z0=50
[difference, index_At_Z0_Equals_50] = min(abs(Z0-50));
% let x_optimum  as the ratio that corresponds to Z0=50ohms
x_optimum = ratio(index_At_Z0_Equals_50)
s=0:0.00001:S;
  w= (2*x_optimum/(1-x_optimum))*s;
plot(s,w,'b','linewidth',2)
grid
title(' the width of coplanar strip line versus slot width for
Z0=50ohms')
 xlabel('slot width s(mm)')
 ylabel('coplanarstrip line w(mm)')
%end
```

Example A.1
The coplanar line designed in Chapter 02 has the following parameters:
Substrate height h =1.62 mm, relative permittivity $\varepsilon_r = 4.3$. In a new script, writing the following:

```
[Z0,ratio] = Z0_characteristic(4.3,5);
```

The effective relative permittivity $\varepsilon_{eff,thick} = 2.65$ and the optimum ratio $\frac{w}{d} = 0.81$.
The plot of the characteristic impedance versus the ratio $\frac{w}{d}$ and the plot of coplanar strip line w versus slot width for $\frac{w}{d} = 0.81$ are shown below.

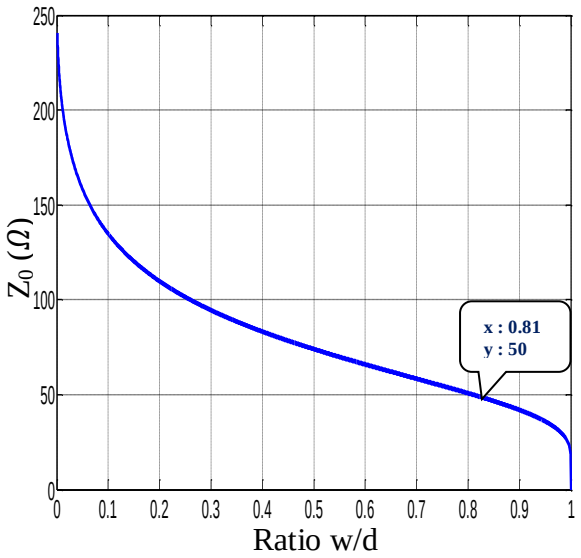

Figure A.2 The characteristic impedance Z_0 versus the ratio $\frac{w}{d}$.

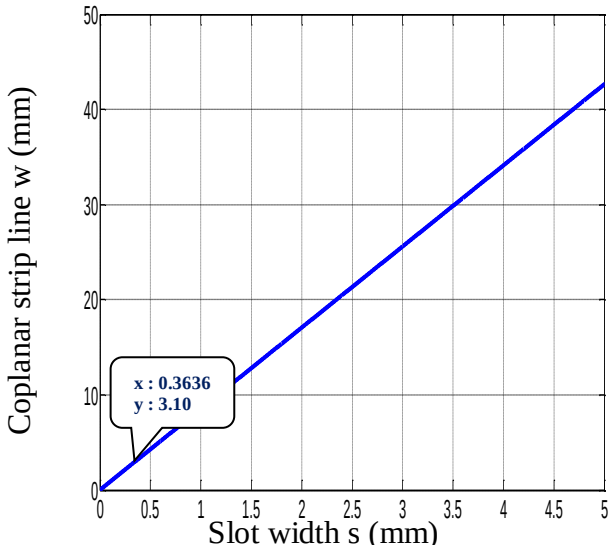

Figure A.3 The width of coplanar strip line versus slot width for $Z_0 = 50\ \Omega$.

Any value from the line shown in figure A.3 will give 50Ω characteristic impedance. For example, $(s, w) = (0.3636, 3.10)$is selected, and verified it using CST SOFTWARE calculator, as shown in Figure A.4:

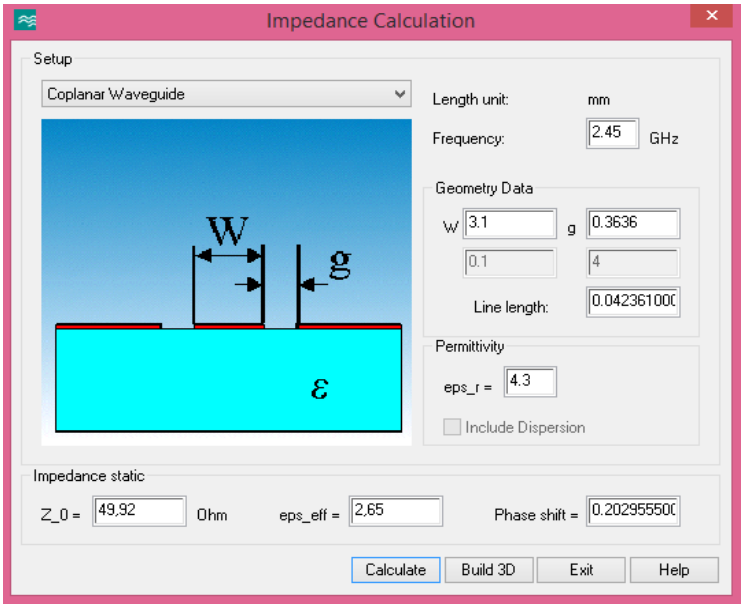

Figure A.4 Impedance coplanar waveguide calculation.